Ellipsoid tether model for collision avoidance in a fleet of ROVs - Full version

Christophe Viel

Ellipsoid tether model for collision avoidance in a fleet of ROVs - Full version

Christophe Viel*

* CNRS, Lab-STICC, F-29806, Brest, France (e-mail: name.surname@ensta-bretagne.fr).

ARTICLE INFO

Keywords:
tether, ROV, cable modeling, collision avoidance, mutli-agent system, umbilical

ABSTRACT

During collision avoidance, the tether of Remote Operated Vehicle (ROV) is subject to entanglement with obstacles or other ROVs' tether. This specificity means that the classic literature on multi-robot obstacles avoidance is not suitable to tethered multi-robot scenarios. This paper proposes a guarantee ellipsoid model of the ROV's tether and its obstacles to perform a collision avoidance method for a fleet of ROVs, low in calculation. This model guarantees that if an obstacle is not inside or partially inside the ellipsoid model, then we are sure that the tether is not collide with that obstacle. This model is simple and can provide a guaranteed proof of non-collision without any knowledge of the tether shape or its dynamic, only its two attachments point and its length. A collision avoidance strategy has been developed based on potential field methods, tether's length management, and bypass path. When several ROVs are involved, personalities are added to ROV to obtain different behaviors in the same configuration and so limit the case of minimal local during collision avoidance. Simulations show the effectiveness of the method with several scenarios and the limits of the method are discussed.

1. Introduction

Remotely Operated Vehicles (ROVs) are underwater robots equipped with a cable, namely umbilical or tether, that connects them to the surface to maintain bi-directional real-time communication, supply the robot with energy, and maintain a lifeline with the robot to avoid losing it. However, this tether has many inconvenient such as collision risks, impact on ROV maneuverability due to cable inertia and drag forces, entanglement, and cable breakage. The problem of entanglement is all the more acute when several ROVs are working in the same area, like for example during pipeline installation [18]. Despite recent progress in obstacle avoidance and trajectory planning for multiple robots and a single tethered robot, the problem of multiple tethered robots trying to reach their individual targets without entanglements remains a challenging problem. Indeed, although there is extensive literature on multi-robot trajectory planning and obstacles avoidance [17, 29, 30, 21, 8, 22], classic methods are often not suitable to tethered multi-robot scenarios.

Most of the studies on the tethered robot planning problem focus on the single robot case and use a representation of homotopy to identify the path or cable configuration [20, 24]. This homotopy approach simplifies the tether configuration by focusing only on the robots' start and end positions, and the tether's position relative to obstacles. Feasible paths are found by exploring a graph augmented with the homotopy classes of the paths. The few works treating the problem of tethered multi-robot [7, 3] applies homotopy theory to determine the path or cable configuration. They induce in most case a slow offline construction of the graph prior obtain an online planning. Note also most of them consider a 2D environment, insufficient to represent the interactions of multiple aerial or underwater robots. Indeed, this technique induces in the vast majority of cases that the cable can be laid on the ground by gravity, allowing flat cables to cross or come into contact with external obstacles [7, 20, 36, 3]. This solution is not possible with underwater tethers: the obstacles are often sharp (sharp-edged rocks, shellfish, corrosion, etc...), the cables evolve in three-dimension because the seabed is not always accessible or cover with obstacles, and crossings between tethers interfere their movements as do the underwater currents. If these solution are promising, the specifics of the cable dynamics must be taken into account when deciding the path.

The tether (or umbilical) of ROV can be modeled by various methods. These range from simple geometrical models like the catenary curve [28, 10, 14] to segment-based models with geometrical constraints [15]. Geometrical models can simulate a large number of segments in real-time and are memory-efficient when precise physical modeling is not necessary. For cases requiring accurate cable dynamics, the Lumped-mass–spring method represents the tether as mass points interconnected by massless elastic elements [16, 19], while the segmental method treats the cable as a continuous system and solves the resulting partial differential equations numerically [12, 13, 4, 6]. However, they require information on the external forces like currents or wave which cannot be easily measured, and sometime a large computation time if an accurate position is required. To take into account all the unknowns and uncertainties, and therefore consider the most unfavorable cases for managing collisions with external obstacles or other cables, an ensemblistic method seems more appropriate.

In this paper, a pessimist but guarantee ellipsoid model of the ROV's tether and its obstacles is proposed to perform a collision avoidance method for a fleet of ROVs, low in calculation. This model guarantees that if an obstacle is not

ORCID(s):

inside or partially inside the ellipsoid model, then we are sure that the tether is not collide with that obstacle. This model is pessimist but can provide a guaranteed proof of non-collision without any knowledge of the tether shape or its dynamic, only its two attachments point and its length.

The aim objectives of this paper is to define

- A simple 3D-model of an un-stretched ROV tether based on ellipsoid for the problem of collision avoidance without any knowledge of the tether shape,
- A collision avoidance method between the different tethers in a fleet of ROVs and the external obstacles based on this model, to reach individual target position,
- The introduction of ROV personality to smooth the collision avoidance between ROVs and solve some local minima.

Since underwater obstacles are often sharp, the possibility of making a bend in the cable with an obstacle is limited or forbidden in this study.

The paper is organized as follow. Section 3 exposes the Problematic, definitions and properties on ellipsoid used in this study. Section 4 presents the model of the tether as an ellipsoid, and the system ROV plus tether as a set of ellipsoids. Section 5 explains how to detect collision between obstacles and the system ROV-tether, then Section 6 proposes the collision avoidance strategies. The path to the ROV's target is chosen in Section 7 to bypass the obstacles directly on the way. Section 8 proposes an algorithm which summarize all the behavior to provide the ROV's motion. Then, Section 9 adds personality in ROVs behavior to solve problem of minima local when several ROVs try to avoid each other. Finally, Section 10 illustrates the results obtains with simulations based on several scenarios in which the number and position of obstacles and ROVs are vary. Limits of the method are discussed.

2. Related Work

2.1. Tether model

The most basics approaches to model tether/umbilical are geometrical models. Cable can be assimulated to catenary curve [28, 14, 10] more or less modified, or neutrally buoyant cables [15] to model them as a series of connected segments. Geometric constraints are incorporated to reflect its stiffness and few dynamic properties. Some elements like ballasts and buoys giving it a predictable shape and assimilated it to straight line, easier to model [33].

For a dynamic and physically accurate cable model, two main types of methods exist as discussed in [4]: the lumped-mass-spring method [16, 19], which represents the tether as a series of mass points linked by massless elastic elements, and the segmental method [12, 13] which treats it as a continuous system and solves the associated partial differential equations numerically. Using Euler-Bernoulli beam theory, cable compression can be represented [13], and some approximation can be performed to use Finite Element Method (FEM) for real-time execution [6]. These methods are suitable for modeling cables dynamic considering external forces like gravity or hydrodynamic drag and bending force, but they often requires significant computational resources and information on the external forces like currents or wave which cannot be measured easily in practice.

The problems of both kind of methods have lead to the solution proposed in Section 4.

2.2. Path-planning and collision avoidance with untether multi-robot

2.2.1. Generality

[8] compares the performance of classic path planing algorithm. Path planning methods of AUV are mainly divided into two categories: global path planning with known static obstacles and local path planning with unknown and dynamic obstacles. If a global map including obstacles is available, global path planning methods can be used to predefined a collision-free path between the starting point and the target point in advance. Algorithms A*, Genetic Algorithm (GA), Ant Colony Algorithm (ACA), Particule Swarm Optimization (PSO), Rapidly-exploring Random Trees (RERT) are global path planning methods. Else, local path planning methods are needed to avoid unknown and dynamic obstacles by obtaining the local environmental information with sensors in real time, on top of a planned path from a global path planner. Common local path planning methods include Artificial Potential Field (APF), Fuzzy Logic (FL), Neural Network (NN) and Reinforcement Learning (RL).

[22] provides a quantitative and qualitative comparisons of path-planning and collision-avoidance systems verified by using numerical tests and also real applications. The presented results show that the most frequently used algorithms tested in the simulated environment are APF, RL, and FL. However, in real implementations, the most frequently used method is the application of behavioral rules based on reacting to changes in the environment in a specific way.

However, very few of these methods study un-tether robots, the cable represents a major constraint in theory and practice.

2.2.2. Artificial Potential Field (APF)

The APF is a navigation technique where robots are guided by virtual forces, attracting them toward goals and repelling them from obstacles [21, 30]. The advantage of the APF is the ease of implementation and low computational requirements, perfect for real time: it is mostly use in swarm of robot [17, 29] where the number of interactions is important. However, this method often struggles with local minima, where robots can become trapped without finding a path to the goal, that's why it is often combine with others methods [23, 35]. Additionally, it may have difficulty navigating narrow spaces or complex environments with closely placed obstacles.

2.2.3. Robot personality

In absence of path planning to plan trajectories or real-time centralized decisions, rules like APF defines the behavior of each robot inside the group, which sometime lead to blocked configuration. Indeed, in multi-robot system, not only cooperation but also competition exists, which may help to improve the efficiency of the system or cause conflict. Thus, some studies like [9, 2, 26, 27] propose to introduce different personalities in the fleet to prevent conflicts by adopting different behavior in a same configuration.

In [9], some "Active" robot moves to avoid obstacle while "Passive" robot stops moving and waits some time before avoiding. Results show the personality strategy has strong adaptability and coordination ability without need to centralize information. [27, 26] investigate on the impact of different "personality types" of robots. It seems that some personalities show significant difference in performance level, while other have virtually no impact on final performance, despite different overall behavior whose usefulness is subjective to the user's needs. Same conclusion is made in [2] which examines the influence of three different "personality types" among drone swarm for a scenario of search and rescue.

2.3. Multi-robot avoidance with tether

Most of the works studying tethered robot planning problem use a representation of homotopy to identify the path or cable configuration. As presented in [20], the homotopy approach consider that two curves connecting the same start and end points are homotopic iff one can be continuously deformed into the other without intersecting any obstacle. Thus, if two cables configuration are homotopic, there exist a path between them. A homotopy augmented graph is so constructed to find the subgraph where the tether shape is reachable from a given position, then the shortest path is found using an A* algorithm. The main problem of these methods is a slow construction of the graph prior obtain an online planning.

Based on this concept, [20, 24] propose an algorithm to find the shortest path for one tether robot from its initial robot-cable configuration to its final robot position, considering also the maximal length of the tether. [3] solves the same problem but with a cable attached at each end to a mobile robots. Few studied like [7] proposes a non-entangling trajectory planning for multiple tethered robots with presence of obstacles. Without homotopy, [36] proposes a plan coordinated motions for tethered mobile robots, avoiding cable entanglement. This method requires to keep the tether taut and retractable: it gives a geometrical shape to the tether with can be assimilated to strait lines with angles when the cable is bend by an obstacle or another robot.

All these work consider a 2D case, making the representation insufficient for capturing the interactions of multiple aerial or underwater robots, and inducing that the cable can be laid on the ground, allowing flat cables to cross or come into contact with external obstacles [7, 20, 36, 3, 24].

3. Problematic and definition

3.1. Notations

Consider the referential $\mathcal{R}$ the global referential. For a variable x, let note $x_{\mathcal{R}_b}$ the variable in a referential $\mathcal{R}_b$. In order to lighten notations, the notations $v_{\mathcal{R}_b} = \begin{bmatrix} x_{\mathcal{R}_b} & y_{\mathcal{R}_b} & z_{\mathcal{R}_b} \end{bmatrix}^T$ and $v_{\mathcal{R}_b} = \begin{bmatrix} x & y & z \end{bmatrix}^T_{\mathcal{R}_b}$ are equivalent. By default, parameters are expressed in $\mathcal{R}$ ($x_{\mathcal{R}}$ is noted x).

3.2. Problematic

The main objective of this study is to lead a ROV i from an initial position to a target objective R_i^* (or a sub-target $\widehat{R}_i^*$) without itself or its tether comes in collision with an other tether or an obstacle. Since tether shape can be complex and an accurate model requires the knowledge of a lot of parameter and sometime a long calculation time, we propose to model tether and other obstacles by ellipsoids. Since ellipsoids don't intersect each other, no collision are possible. This section proposes tools link to ellipsoid which will be used in the rest of this study.

3.3. Definition of ellipsoid

In this work, ellipsoids are used to model the tether and the obstacles in the environment. This section exposes the main notations and properties about ellipsoid used in this paper.

Definition 1. *Let a_i, b_i and c_i be the length of the semi-axes of the ellipsoid $\mathcal{E}_i$ and $C_i = \left[x_{c,i}, y_{c,i}, z_{c,i}\right]^T_{\mathcal{R}}$ be the center of $\mathcal{E}_i$. Let's note $\vec{a}_i$, $\vec{b}_i$ and $\vec{c}_i$ the **normalized** three axes that intersect at the center C_i and consider a_i is the longest axis of $\mathcal{E}_i$, called "**main semi-axis**". The general expression of an ellipsoid $\mathcal{E}_i$ in its own referential $\mathcal{R}_i = \left(C_i, \vec{a}_i, \vec{b}_i, \vec{c}_i\right)$ can be defined as*

$$\frac{x^2_{\mathcal{R}_i}}{a_i^2} + \frac{y^2_{\mathcal{R}_i}}{b_i^2} + \frac{z^2_{\mathcal{R}_i}}{c_i^2} = 1. \tag{1}$$

*Let also define $F_{1,i} = C_i - \vec{a}_i$ and $F_{2,i} = C_i + \vec{a}_i$ the two focals of $\mathcal{E}_i$, and $\vec{d}_i = \vec{F_{1,i}F_{2,i}}$ be the "**main axis**".*

In the frame of reference $\mathcal{R}$, the ellipsoid $\mathcal{E}_i$ can be expressed with the matrix form

$$0 = \bar{X}^T \boldsymbol{M_b}^i \bar{X} \tag{2}$$

where $\bar{X} = \begin{bmatrix} x & y & z & 1 \end{bmatrix}^T_{\mathcal{R}}$, $\boldsymbol{M_b}^i = \boldsymbol{T}\boldsymbol{M_a}^i\boldsymbol{T}^T$ and

$$\boldsymbol{M_a}^i = \begin{bmatrix} \boldsymbol{A} & \boldsymbol{D} & \boldsymbol{E} & \boldsymbol{G} \\ \boldsymbol{D} & \boldsymbol{B} & \boldsymbol{F} & \boldsymbol{H} \\ \boldsymbol{E} & \boldsymbol{F} & \boldsymbol{C} & \boldsymbol{J} \\ \boldsymbol{G} & \boldsymbol{H} & \boldsymbol{J} & \boldsymbol{K} \end{bmatrix} \tag{3}$$

$$\boldsymbol{T} = \begin{bmatrix} 1 & 0 & 0 & 0 \\ 0 & 1 & 0 & 0 \\ 0 & 0 & 1 & 0 \\ -x_{c,i} & -y_{c,i} & -z_{c,i} & 1 \end{bmatrix}. \tag{4}$$

where $\boldsymbol{A}, \boldsymbol{B}, \boldsymbol{C}, \boldsymbol{D}, \boldsymbol{E}, \boldsymbol{F}, \boldsymbol{G}, \boldsymbol{H}, \boldsymbol{J}, \boldsymbol{K}$ *are constant.*

Finally, let define $\boldsymbol{M_c}^i$ *the transformation matrix between* $\mathcal{R}$ *and* $\mathcal{R}_i$ *such that*

$$X_{\mathcal{R}_i} = \boldsymbol{M_c}^i \left(X_{\mathcal{R}} - C_{i|\mathcal{R}} \right). \tag{5}$$

In this paper, a particular case of ellipsoid such that $b_i = c_i$, named ellipsoid of revolution, is mostly used. Their particularities are described in Definition 2.

Definition 2. *Consider the particular case of ellipsoid of revolution where* $b_i = c_i$. *In the main referential* $\mathcal{R}$, *let define* $F_{1,i} = \left[x_{F_1,i}, y_{F_1,i}, z_{F_1,i}\right]^T$ *and* $F_{2,i} = \left[x_{F_2,i}, y_{F_2,i}, z_{F_2,i}\right]^T$ *the coordinate of the two focal of* $\mathcal{E}_i$, *supposed known. The orientation of the main semi-axis* $\vec{a}_i$ *in* $\mathcal{R}$ *can be expressed with the rotation of angles* θ_i *and* ψ_i *around* $C_i\vec{b}_i$ *and* $C_i\vec{c}_i$ *such that*

$$\theta_i = atan2\left(y_{F_2,i} - y_{F_1,i}, x_{F_2,i} - x_{F_1,i}\right) \tag{6}$$

$$\psi_i = \begin{cases} asin\left(\frac{z_{F_2,i} - z_{F_1,i}}{\|F_{1,i}F_{2,i}\|}\right) & if\ \|F_{1,i}F_{2,i}\| > 0 \\ 0 & else \end{cases} \tag{7}$$

and the center of the ellipsoid $C_i = \begin{bmatrix} x_{c,i} & y_{c,i} & z_{c,i} \end{bmatrix}^T$ *can be expressed as*

$$C_i = \frac{F_{1,i}\vec{F}_{2,i}}{2} + F_{1,i}. \tag{8}$$

In the frame of reference $\mathcal{R}$, *the ellipsoid* $\mathcal{E}_i$ *can be expressed in the matrix form (2) where* $\boldsymbol{G} = \boldsymbol{H} = \boldsymbol{J} = 0$, $\boldsymbol{K} = -1$ *and*

$$\boldsymbol{A} = \frac{d^2}{a_i^2} + \frac{g^2}{b_i^2} + \frac{j^2}{c_i^2} \quad \boldsymbol{B} = \frac{e^2}{a_i^2} + \frac{h^2}{b_i^2} + \frac{k^2}{c_i^2}$$
$$\boldsymbol{C} = \frac{f^2}{a_i^2} + \frac{i^2}{b_i^2} + \frac{l^2}{c_i^2} \quad \boldsymbol{D} = \frac{de}{a_i^2} + \frac{gh}{b_i^2} + \frac{jk}{c_i^2}$$
$$\boldsymbol{E} = \frac{df}{a_i^2} + \frac{gi}{b_i^2} + \frac{jl}{c_i^2} \quad \boldsymbol{F} = \frac{ef}{a_i^2} + \frac{hi}{b_i^2} + \frac{kl}{c_i^2}$$

with $d = \cos\left(\theta_i\right)\cos\left(\psi_i\right)$, $e = \cos\left(\theta_i\right)\sin\left(\psi_i\right)$, $f = \sin\left(\theta_i\right)$, $g = -\sin\left(\psi_i\right)$, $h = \cos\left(\psi_i\right)$, $i = 0$, $j = -\sin\left(\theta_i\right)\cos\left(\psi_i\right)$, $k = -\sin\left(\theta_i\right)\sin\left(\psi_i\right)$, $l = \cos\left(\theta_i\right)$. *Moreover, in (5), the transformation matrix* $\boldsymbol{M_c}^i$ *between* $\mathcal{R}$ *and* $\mathcal{R}_i$ *can be expressed as*

$$\boldsymbol{M_c}^i = \begin{bmatrix} d & e & f \\ g & h & i \\ j & k & l \end{bmatrix}. \tag{9}$$

Details of Definition 2 are available in the Appendix B.1.

3.4. Intersection between two ellipsoids

The following Theorem 1 allows to find if two ellipsoids $\mathcal{E}_i$ and $\mathcal{E}_j$ intersect or not.

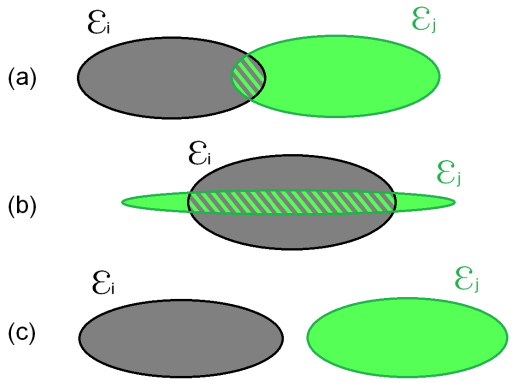

Figure 1: Intersection between ellipsoids $\mathcal{E}_i$ and $\mathcal{E}_j$. (a): just intersect; (b) ellipsoid $\mathcal{E}_j$ fully crosses the ellipsoid $\mathcal{E}_i$; (c) $\mathcal{E}_i$ and $\mathcal{E}_j$ not intersected.

Theorem 1. *[1] Let's define two ellipsoids* $\mathcal{E}_i$ *and* $\mathcal{E}_j$ *with the associated two matrices* $\boldsymbol{M_b}^i$ *and* $\boldsymbol{M_b}^j$ *as described in (3) in Definition 1. We define* $\lambda^{ij} = \left[\lambda_k^{ij}\right]$ *with* $k = [1, \dots, 4]$ *the vector of eigenvalues of the matrix* $\boldsymbol{M}^{ij} = \left(\boldsymbol{M_b}^i\right)^{-1}\boldsymbol{M_b}^j$. *It can be shown that*

(1) If one of the eigenvalues λ_k^{ij} *have an imaginary part, i.e.* $\exists k \in [1, \dots, 4]$ *such that* $Im\left(\lambda_k^{ij}\right) \neq 0$, *then* $\mathcal{E}_i$ *and* $\mathcal{E}_j$ *intersect without one ellipsoid crossing the other completely, see Figure 1(a);*

(2) If all eigenvalues λ_k^{ij} *are real positive, i.e.* $\forall k \in [1, \dots, 4]$ *one has* $Im\left(\lambda_k^{ij}\right) = 0$ *and* $Re\left(\lambda_k^{ij}\right) \geq 0$, *then* $\mathcal{E}_i$ *and* $\mathcal{E}_j$ *intersect and one ellipsoid crosses the other completely, see Figure 1(b);*

(3) Else, there is not intersection between $\mathcal{E}_i$ *and* $\mathcal{E}_j$ *or the two are perfectly superposed, i.e.* $\mathcal{E}_i \cap \mathcal{E}_j = \emptyset$ *if* $\mathcal{E}_i \neq \mathcal{E}_j$.

In case (1) and (2), one has $\mathcal{E}_i \cap \mathcal{E}_j \neq \emptyset$.

Proof of Theorem 1 is described in [1] (note that the notations used in [1] are different).

4. Tether model

4.1. Tether ellipsoid model

In this study, a tether i is assimilated to a cable characterized by the three parameters L_i,O_i and R_i where

- $R_i = \left[x_{R,i}, y_{R,i}, z_{R,i}\right]^T$ is the first extremity of the tether, here the ROV position;
- $O_i = \left[x_{O,i}, y_{O,i}, z_{O,i}\right]^T$ is the second extremity of the tether, which can be a surface vessel, another underwater vehicle, a TMS, a cage or an anchor at the extremity of another cable;
- $L_i(t) \in \left[0, L_{i,\max}\right]$ is the length of the tether, whose length may vary using possible TMS positioned on R_i or O_i. Let define $\delta L_{\max}$the length of cable that can be reduced/extended during a fixed time $\Delta T > 0$, where

$\delta L_{\max}$ can be the mechanical limit of the TMS or a chosen parameter.

In the rest of the study, let's call O_i an "anchor" and R_i an "ROV". We suppose that

A1) the extremity O_i is supposed to be fixed.

A2) the extremities R_i is strong enough to compensate action of the cables, therefore remain stationary since an operator doesn't decide to move on of theses points.

A3) The parameters O_i, R_i and $L_i(t)$ are supposed supposed to be known,

A4) Excepted the three parameters L_i,O_i and R_i, we have no information on the tether i. This includes its shape, its rigidity, its dynamics, its weight or buoyancy, the forces applied on it like the underwater currents, etc...

In absence of information on the tether as described Assumption A4, we desire to find a shape that wraps the cable in all circumstances to guarantee the absence of collision with its environment. Based on the gardener's method to draw ellipse, the tether i can draw an ellipsoid $\mathcal{E}_i$ corresponding to the maximum distances it can reach, where O_i and R_i are the two stakes. Thus tether i is always inside this associated ellipsoid $\mathcal{E}_i^L$, see examples on Figure 2. Characteristic of this ellipsoid are described in Definition 3.

Definition 3. *The tether i is include inside the ellipsoid of revolution $\mathcal{E}_i^L$ as defined in Definition 2 with the following parameters*

$$a_i = \frac{L_i}{2} \tag{10}$$

$$b_i = \sqrt{\left(\frac{L_i}{2}\right)^2 - \left(\frac{d_i}{2}\right)^2} \tag{11}$$

$$c_i = b_i \tag{12}$$

$$d_i = \left\|O_i R_i\right\| \tag{13}$$

*where $\frac{\vec{a}_i}{\|\vec{a}_i\|} = \frac{\vec{d}_i}{\|\vec{d}_i\|}$. Note that a_i is the "**main semi-axis**" of $\mathcal{E}_i$ and d_i is the "**main axis**" as defined in Definition 1 because $a_i \geq b_i$ and $b_i = c_i$. Note that $d_i \leq L_i$ since the ROV cannot go further that the tether length. The two focal of $\mathcal{E}_i^L$ are $F_1 = O_i$ and $F_2 = R_i$, so $C_i = \frac{\vec{O_i R_i}}{2} + O_i$ and so one has*

$$\theta_i = atan2\left(y_{R,i} - y_{O,i}, x_{R,i} - x_{O,i}\right) \tag{14}$$

$$\psi_i = \begin{cases} asin\left(\frac{z_{R,i} - z_{O,i}}{d_i}\right) & if\ d_i > 0 \\ 0 & else \end{cases} \tag{15}$$

The proof and calculation of all parameters in Definition 3 is described in Appendix B.2.

This ellipsoidal model provides a guarantee area where the tether cannot be outside. The shape of $\mathcal{E}_i^L$ can be partially controlled by 1) the distance between ROV R_i and anchor O_i ($\mathcal{E}_i^L$ is a sphere if $O_i = R_i$); 2) reducing/extending the the length L_i.

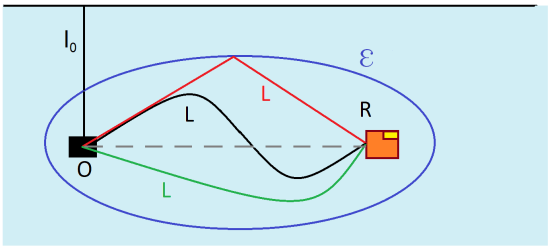

Figure 2: Examples of tethers shapes in their associated ellipsoids $\mathcal{E}$. For each ellipsoid, three example of tether shape (red, black and green). Here, O_i is an anchor. Note the cable l_0 can be equal to zero.

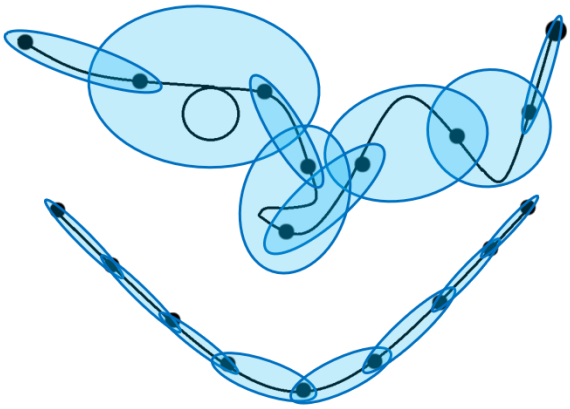

Figure 3: Examples of tethers shapes assimilated to several ellipsoids if the position of several point (black dots) are known. This method is not used in the rest of the paper.

Remark 1. *In the same way, if the position of several points on the tether are known, then the cable can be assimilated to several smallest ellipsoid, as illustrated in Figure 3. In this paper, only O_i and R_i are supposed to be known.*

4.2. System "Anchor-Tether-ROV" $\mathcal{S}_i$

Depending of their positions, the two attachment point O_i and R_i (name it "ROV" and "anchor") are not necessary enclosed within $\mathcal{E}_i^L$ and can be subject to entanglement with other tether/ROV j working in the same area. Thus, we propose to model them by ellipsoids $\mathcal{E}_i^R$ and $\mathcal{E}_i^O$ as illustrated in Figure 4 such that:

A5) items at positions R_i and O_i can be enclosed inside ellipsoids $\mathcal{E}_i^R$ and $\mathcal{E}_i^O$, center in R_i and O_i, following the Definition 1.

A6) Let $\mathcal{S}_i$ be the system "Anchor-Tether-ROV" of ROV i which can be modeled by the set of ellipsoid $\mathcal{S}_i = \left\{\mathcal{E}_i^L, \mathcal{E}_i^R, \mathcal{E}_i^O\right\}$. The potential collisions/ entanglements between $\mathcal{E}_i^L$ and $\mathcal{E}_i^R$ or $\mathcal{E}_i^O$ are not considered in this paper.

Note that $\mathcal{E}_i^R$ and $\mathcal{E}_i^O$ can be spheres or chosen ellipsoids of revolution as defined in Definition 2. Let's define $\mathcal{L}_{\mathcal{S}} = \left\{\mathcal{S}_1, \ldots, \mathcal{S}_N\right\}$ the list of systems $\mathcal{S}_i$. The tether is inside the guarantee area $\mathcal{S}_i$ such that if an obstacle is not inside or

doesn't intersect with $\mathcal{S}_i$, then we are sure that the tether is not collide with that obstacle. Else, no conclusion can be made except there is a risk of collision. This model is pessimist because depending of the position of the focal O_i and R_i the ellipsoid can be very imposing, but it can provide a guaranteed proof of non-collision without any knowledge of the tether shape. Some strategies in Sections 5.2 and 6 will propose methods to reduce the pessimism or the volume of $\mathcal{S}_i$.

4.3. ROV motion model

The objective of this paper is not to model the ROV but the system $\mathcal{S}_i$ Anchor-Tether-ROV. Since the anchor O_i is supposed immobile, the ROV is the only actuator of $\mathcal{S}_i$ which changes its shape and position by moving R_i. We focus here on the motion control of R_i using the following discrete model:

$$R_i\left(t_{k+1}\right) = \Delta T\left(\alpha_{R_i}\left(t_k\right) V_{R_i\max}\vec{v}_{R_i}\left(t_k\right)\right) + R_i\left(t_k\right) \tag{16}$$

where $\Delta T > 0$ is the sampling time, $V_{R_i\max} > 0$ is the absolute maximum velocity of the ROV i, $\alpha_{R_i}(t) \in [0,1]$ a velocity ratio, and $\vec{v}_{R_i}(t)$ with $\left\|\vec{v}_{R_i}\right\| = 1$ the unitary direction vector of the motion of R_i at an instant $t > 0$. We suppose that the ROV has already a controller 1) to follow $V_{R_i} = \alpha_{R_i} V_{R_i\max}$ and $\vec{v}_{R_i}$ (field-oriented control input), or 2) to reach the point $R_i\left(t_{k+1}\right)$ from $R_i\left(t_k\right)$ during time ΔT.

In the same way, let's define $\hat{R}_i\left(t_{k+1}, \alpha, \vec{v}\right)$ the estimation of $R_i\left(t_{k+1}\right)$ at an instant t_k for chosen α_{R_i} and $\vec{v}_{R_i}$ such as

$$\hat{R}_i\left(t_{k+1}, \alpha_{R_i}, \vec{v}_{R_i}\right) = \Delta T\left(V_{R_i\max}\alpha_{R_i}\vec{v}_{R_i}\right) + R_i\left(t_k\right). \tag{17}$$

Parameters α_{R_i} and $\vec{v}_{R_i}$ will depend of the target of the ROV and the obstacle avoidance strategy, detailed in next sections.

5. Detection obstacle collision

5.1. Classification of obstacles

The obstacles j of an system $\mathcal{S}_i$ are also modeled by ellipsoids, divided in three categories:

- **Full obstacle:**

An irregular shape object which can be contained inside an ellipsoid $\mathcal{E}_k$ as defined in Definition 1, see Figure 4. These obstacles are considered "untouchable" (sharp, risk of snagging, dangerous, etc...), and so no intersection between $\mathcal{E}_k$ and $\mathcal{S}_i$ is allowed. Let $\mathcal{L}_\mathcal{O} = \left\{\mathcal{O}_1, \ldots, \mathcal{O}_M\right\}$ be the list of full obstacle $\mathcal{O}_m$ with $m \in \mathcal{M} = \{1, \ldots, M\}$.

- **Tether obstacle:**

An other system $\mathcal{S}_j$, a tether/cable or an obstacle as it will be defined in Section 4.2. Let $\mathcal{L}_\mathcal{S} = \left\{\mathcal{S}_1, \ldots, \mathcal{S}_N\right\}$ be the list of potential tethers obstacles $\mathcal{S}_n$ (including ROVs) with $n \in \mathcal{M} = \{1, \ldots, N\}$, and $\mathcal{L}_\mathcal{S}^{(-i)} = \left\{\mathcal{L}_\mathcal{S} - \left\{\mathcal{S}_i\right\}\right\}$ be the list of tethers obstacles of $\mathcal{S}_i$, *i.e.* the list $\mathcal{L}_\mathcal{S}$ except $\mathcal{S}_i$ itself. Note that a tether $\mathcal{S}_j$ can also be considered as three full obstacles $\mathcal{O}_m$ as it will be described in Section 5.3.

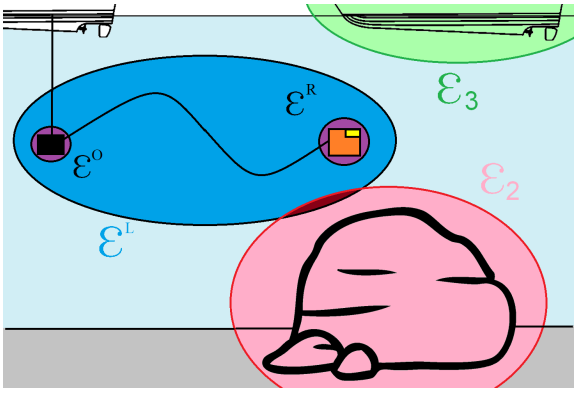

Figure 4: Collision (dark red area) between the ellipsoid $\mathcal{E}^L$ containing the tether and an obstacle inside the ellipsoid $\mathcal{E}_2$. Colored ellipsoids $\mathcal{E}_2$ and $\mathcal{E}_3$ are fixed full-obstacles. Purple: ellipsoids $\mathcal{E}^R$ and $\mathcal{E}^O$ containing the ROV or the anchor.

- **Plane obstacle:**

A plane surface $\mathcal{P}$, to model for example seabed, surface or wall. Let $\mathcal{L}_\mathcal{P}$ be the list of all a plane obstacle $\mathcal{P}_k$ with $k \in \mathcal{K} = \{1, \ldots, K\}$.

Then, let $\mathcal{L}^i_{\text{obs}}$ be the list of obstacles of the system $\mathcal{S}_i$ such that $\mathcal{L}^i_{\text{obs}} = \left\{\mathcal{L}_\mathcal{O}, \mathcal{L}_\mathcal{S}^{(-i)}, \mathcal{L}_\mathcal{P}\right\}$. The number of elements of $\mathcal{L}^i_{\text{obs}}$ is $N_{\text{obs}} = N - 1 + M + K$. Let also define $\mathcal{A}^i_j$ as an generic obstacle of $\mathcal{S}_i$ such that $\mathcal{A}^i_j = \mathcal{L}^i_{\text{obs}}(j)$ with $j \in \left\{1, \ldots, N_{\text{obs}}\right\}$.

Let's define $\mathcal{L}^i_\mathcal{Q} = \left\{Q_{i1}, \ldots, Q_{iN_{\text{obs}}}\right\}$ the list of collisions of $\mathcal{S}_i$ where $Q_{ij} \in \{0 \ldots 4\}$ defines the type of collisions between $\mathcal{S}_i$ and $\mathcal{A}^i_j \in \mathcal{L}^i_{\text{obs}}$, as described below:

1. $Q_{ij} = 0$ if $\mathcal{S}_i \cap \mathcal{A}^i_j = \emptyset$;
2. $Q_{ij} = 1$ if $\mathcal{E}^O_i \cap \mathcal{A}^i_j \neq \emptyset$;
3. $Q_{ij} = 2$ if $\mathcal{E}^R_i \cap \mathcal{A}^i_j \neq \emptyset$;
4. $Q_{ij} = 3$ if $\mathcal{E}^L_i \cap \mathcal{A}^i_j \neq \emptyset$, except particular cases described in Section 5.3;
5. $Q_{ij} = 4$ if there is a **"crossing collision"** between two tethers $\mathcal{E}^L_i$ and $\mathcal{E}^L_j$, as it will be described in Section 5.3.

Finally, let's give the definition of a fixed obstacle.

Definition 4. *A **fixed obstacle** is an obstacle which can/will not move. An ROV which has reached its target position R^*_i is considered as a fixed obstacle.*

Depending of the obstacle categories, different tests are proposed to detect the collision and the type of collision Q_{ij}. Theses tests are described in the following subsections.

5.2. Full obstacle

The "full obstacles" are items which can be enclosed inside an ellipsoid $\mathcal{E}_k$. Its can be for example a rock, a boat, an ROV, an anchor, a submarine structure, etc... see Figure 4. Encapsulate them in ellipsoid allows us to generalize their very diverse shapes by dealing only with collisions between ellipsoids. Indeed, if there is not intersection between two ellipsoids each containing an item, then there is not possible collision between them, see Theorem 2.

Theorem 2. *Consider two geometric volumes V_i and V_j which can be contained respectively inside ellipsoids $\mathcal{E}_i$ and $\mathcal{E}_j$, i.e. $V_i \subset \mathcal{E}_i$ and $V_j \subset \mathcal{E}_j$. If there is not intersection between $\mathcal{E}_i$ and $\mathcal{E}_j$, i.e. $\mathcal{E}_i \cap \mathcal{E}_j = \emptyset$, them there is not intersection (and so collision) possible between S_i and S_j, i.e $V_i \cap V_j = \emptyset$.*

The proof of Theorem 2 is obvious: If $V_i \subset \mathcal{E}_i$, $V_j \subset \mathcal{E}_j$ and $\mathcal{E}_i \cap \mathcal{E}_j = \emptyset$, then $V_i \cap V_j = \emptyset$.

Based on Theorem 2 and since the system S_i is composed of three ellipsoids, one can make the following Theorem 3.

Theorem 3. *There is no collision between the system S_i and an obstacle $\mathcal{E}_k$ if the three conditions $\mathcal{E}_i^L \cap \mathcal{E}_k = \emptyset$, $\mathcal{E}_i^O \cap \mathcal{E}_k = \emptyset$ and $\mathcal{E}_i^R \cap \mathcal{E}_k = \emptyset$ are respected. In this case, let's note $S_i \cap \mathcal{E}_k = \emptyset$. Else, let's note $S_i \cap \mathcal{E}_k \neq \emptyset$, and a collision is possible.*

One takes $Q_{ij} = \max\left(\left[q_1, q_2, q_3\right]\right)$ where $q_1 = 1$ if $\mathcal{E}_i^O \cap \mathcal{E}_k \neq \emptyset$, $q_1 = 0$ else; $q_2 = 2$ if $\mathcal{E}_i^R \cap \mathcal{E}_k \neq \emptyset$, $q_2 = 0$ else; and $q_3 = 3$ if $\mathcal{E}_i^L \cap \mathcal{E}_k \neq \emptyset$, $q_3 = 0$ else.

Same proof that for Theorem 2 with $\mathcal{E}_i^R$ and $\mathcal{E}_i^O$.

The most difficult part is to show that there is no intersection between the two ellipsoids $\mathcal{E}_i$ and $\mathcal{E}_j$: the Theorem 1 presented in Section 3.4 provides a solution to test this condition.

Using the Theorems 1, 2 and 3, the collision between S_i and an full obstacle can be detected.

5.3. Tether obstacles

5.3.1. Tether system obstacle detection

Checking the collision between two systems S_i and S_j by considering their ellipsoids as full obstacles is very pessimistic because the effective volume occupied by the tether *i* is sometime much smaller than $\mathcal{E}_i^L$. Moreover, it can be observed that the risk of entanglement between the two cables appears only when:

- (a) there is a risk of snagging when the tether *i* is in contact with 1) ROV R_j or anchor O_j ; 2) objects attached to cable *j* (ballast, buoy, sensor, etc...); 3) the tether *j* if it is naturally twisted. Same with tether *j*.
- (b) the end O or R passes inside a loop, risking of creation of a knot (see Figure 5(b)). The formation of a knot is uncommon if neither end is involved, see Figure 5(a);
- (c) one cable tries to pass between the two ends of the other tether, see Figure 5(c): during its displacement, neither O_i or R_i come inside $\mathcal{E}_j^L$, but the tether *i* crosses $\mathcal{E}_j^L$ and so make an entanglement.

In the case (a), each element of S_j must be considered as three full obstacles as described in Section 5.2. Else, a less restrictive alternative is proposed where a collision between S_i and S_j happens in the two following cases:

- **"Intrusion collision"**: $\mathcal{E}_i^O$or $\mathcal{E}_i^R$ comes in collision with $\mathcal{E}_j^L$, $\mathcal{E}_j^O$or $\mathcal{E}_j^R$, see Figure 5(b). Same conditions for S_j withS_i.
- **"Crossing collision"**: Between two instants t_k and t_{k+1}, one cable has passed between the two ends of the other tether, see Figure 5(c), *i.e.* $\exists t \in \left[t_k, t_{k+1}\right]$ such that $\left[O_i R_i\right](t) \cap \left[O_j R_j\right](t) \neq \emptyset$:

Note that the crossing collision depends of the previous positions, because its new position could have been reached without creating entanglement if one tether had bypassed the other tether without crossing it.

Two theorems are defined to test the collision between two tethers.

Theorem 4. ***"intrusion collision"**. There is no collision of type "intrusion" between the two systems S_i and S_j if $\hat{\mathcal{E}}_i \cap S_j = \emptyset$ and $\hat{\mathcal{E}}_j \cap S_i = \emptyset$ where $\hat{\mathcal{E}}_\ell = \left\{\mathcal{E}_\ell^R, \mathcal{E}_\ell^O\right\}$ with $\ell \in \{i, j\}$. In this case, let's note $S_i \cap S_j = \emptyset$. Else, let's note $S_i \cap S_j \neq \emptyset$, and a collision is possible.*

One takes $Q_{ij} = \max\left(\left[q_1, q_2, \hat{q}_3, \tilde{Q}_{ij}(t)\right]\right)$ where $q_1 = 1$ if $\mathcal{E}_i^O \cap S_j \neq \emptyset$, $q_1 = 0$ else; and $q_2 = 2$ if $\mathcal{E}_i^R \cap S_j \neq \emptyset$, $q_2 = 0$ else; $\hat{q}_3 = 3$ if $\mathcal{E}_i^L \cap \hat{\mathcal{E}}_j \neq \emptyset$, $\hat{q}_3 = 0$ else; and where $\tilde{Q}_{ij}(t)$ is defined in Theorem 5.

Same element of proof that for Theorem 2. Note that $\mathcal{E}_i^L \cap \mathcal{E}_j^L \neq \emptyset$ doesn't lead to $S_i \cap S_j \neq \emptyset$ *or* $Q_{ij} > 0$.

Theorem 5. ***"crossing collision"**. For an instant $t > 0$, let $\bar{S}_i(t) \in \left[O_i R_i\right](t)$ and $\bar{S}_j(t) \in \left[O_j R_j\right](t)$ be the closest points between the two main axis of ellipsoids $\mathcal{E}_i^L(t)$ and $\mathcal{E}_j^L(t)$. Let define the vector $\vec{v_{ij}}(t) = \bar{S}_j(t) - \bar{S}_i(t)$. Consider two instants t_k and t_{k+1} such that $0 < t_k < t_{k+1}$ with $\left|\left\|\vec{v_{ij}}\left(t_k\right)\right\| - \left\|\vec{v_{ij}}\left(t_{k+1}\right)\right\|\right| < \varepsilon$ where $\varepsilon > 0$ is relatively small. Finally, consider a memory variable $\tilde{Q}_{ij}(t)$ such that $\tilde{Q}_{ij}(t) = 0$ if no crossing collision have detected, $\tilde{Q}_{ij}(t) = 4$ else.*

(1) Suppose there is no crossing collision at instant t_k, i.e. $\tilde{Q}_{ij}\left(t_k\right) = 0$. If $\vec{v_{ij}}\left(t_{k+1}\right).\vec{v_{ij}}\left(t_k\right) \leq 0$, the segments $\left[O_i R_i\right](t)$ and $\left[O_j R_j\right](t)$ have crossed: one takes $\tilde{Q}_{ij}\left(t_{k+1}\right) = 4$. Else, they are still in in the same side and one keeps $\tilde{Q}_{ij}\left(t_{k+1}\right) = \tilde{Q}_{ij}\left(t_k\right)$.

(2) Suppose there is crossing collision at instant t_k , i.e. $\tilde{Q}_{ij}\left(t_k\right) = 4$. If $\vec{v_{ij}}\left(t_{k+1}\right).\vec{v_{ij}}\left(t_k\right) \leq 0$, the segments $\left[O_i R_i\right](t)$ and $\left[O_j R_j\right](t)$ are not crossed anymore: one takes $\tilde{Q}_{ij}\left(t_{k+1}\right) = 0$. Else, they are still crossed and one keeps $\tilde{Q}_{ij}\left(t_{k+1}\right) = \tilde{Q}_{ij}\left(t_k\right)$.

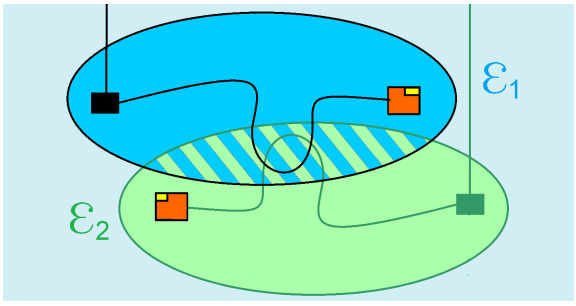

(a) The two ellipsoids are in contact with few risk of entanglement as long as ROVs stay outside the ellipsoid of the other tether and do not pass completely through the other ellipsoid.

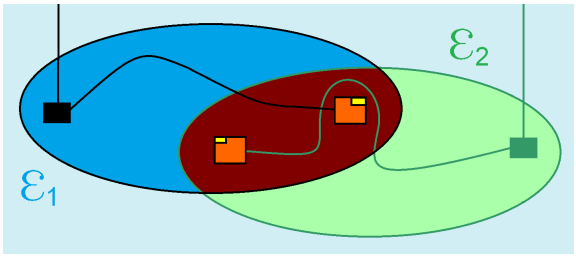

(b) ROVs inside the ellipsoid of the other tether: risk of entanglement.

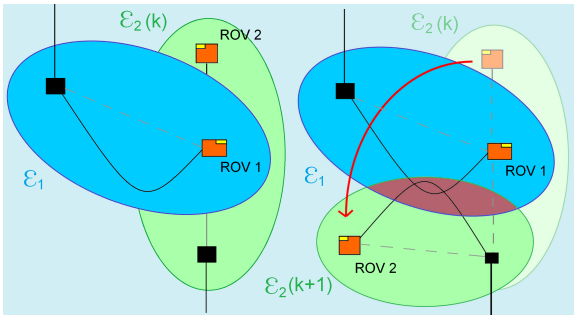

(c) During its displacement, the ROV 2 does not come inside $\mathcal{E}_1$, but its tether crosses $\mathcal{E}_1$ and so make an entanglement.

Figure 5: Intersection between tether $\mathcal{E}_1$ (in blue) and $\mathcal{E}_2$ (in green), supposed assumed without attached item and untwisted. In brown: risk of entanglement.

The proof of Theorem 5 is provided in Appendix B.3. The Theorem 10 in Appendix A.1 proposes a method to evaluate $\bar{S}_i(t)$ and $\bar{S}_j(t)$.

5.3.2. *System obstacle* $\mathcal{S}_j$

An obstacle $\mathcal{O}_j$ can be assimilated to a system $\mathcal{S}_j = \left\{\mathcal{E}_j^L, \mathcal{E}_j^R, \mathcal{E}_j^O\right\}$ if

- The non-convex parts of $\mathcal{O}_j$ are inside $\mathcal{E}_j^O$ or $\mathcal{E}_j^R$;
- The volume of $\mathcal{O}_j$ which is not inside $\mathcal{E}_j^O$ or $\mathcal{E}_j^L$ is 1) convex and the tether can bend around it without risk of snagging or cutting; 2) can be included in a ellipsoid of revolution $\mathcal{E}_j^L$ with the focal F_1 and F_2 corresponding to the center of $\mathcal{E}_j^O$ and $\mathcal{E}_j^R$.

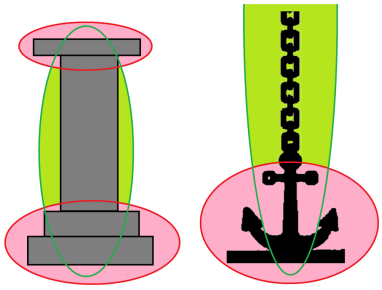

Figure 6: Example of system obstacle $\mathcal{S}_j$. Pink: ellipsoid $\mathcal{E}_j^O$ or $\mathcal{E}_j^R$ containing a forbidden area for the tether. Green: ellipsoid $\mathcal{E}_j^L$ containing a surface where the tether can bend with risk.

The obstacle $\mathcal{O}_j$ can be another underwater cable, but also a smooth surface that connects an uncorroded pillar or pipe, as illustrated in Figure 6. This model allows small bend between the tether and an obstacle, and reduce drastically the volume of the obstacle modeled. The system obstacle are included in the list $\mathcal{L}_\mathcal{S}$ and follow the rules than defined in Section 5.3.1.

5.4. Plane obstacle

The planes obstacles $\mathcal{P}_k$ can model for example seabed, surface or wall. In this paper, theorems and definition consider only infinite planes. Note that these surface are rarely smooth (rocks, seaweed, floating objects...), so we consider there is a risk of hooking and clipping if the tether comes in collision with the plane that covers the hazardous surface.

Definition 5. *A plane $\mathcal{P}_k$ can be defined by its normal vector $\vec{n}_k = \begin{bmatrix} \alpha_k & \beta_k & \gamma_k \end{bmatrix}^T$ and a point $P_k = \left[x_{P,k}, y_{P,k}, z_{P,k}\right]^T$. Let's note it $\mathcal{P}_k\left(P_k, \vec{n}_k\right)$.*

$\mathcal{P}_k$ can be expressed by the following equation

$$\alpha_k x + \beta_k y + \gamma_k z + \delta_k = 0 \tag{18}$$

where $\delta_k = -\left(\alpha_k x_{P,k} + \beta_k y_{P,k} + \gamma_k z_{P,k}\right)$.

The collision between a system $\mathcal{S}_i$ and a plane $\mathcal{P}_k$ can happen if 1) the ROV R_i comes in collision with the plane, 2) the tether itself touch the plane. These conditions are expressed in Theorem 6.

Theorem 6. *There is no collision between the tether system $\mathcal{S}_i$ and an plane $\mathcal{P}_k$ if the three conditions $\mathcal{E}_i^L \cap \mathcal{P}_k = \emptyset$, $\mathcal{E}_i^O \cap \mathcal{P}_k = \emptyset$ and $\mathcal{E}_i^R \cap \mathcal{P}_k = \emptyset$ are respected. In this case, let's note $\mathcal{S}_i \cap \mathcal{P}_k = \emptyset$. Else, let's note $\mathcal{S}_i \cap \mathcal{P}_k \neq \emptyset$, and a collision is possible.*

One has $Q_{ij} = \max\left(\left[q_1, q_2, q_3\right]\right)$ where $q_1 = 1$ if $\mathcal{E}_i^O \cap \mathcal{P}_k \neq \emptyset$, $q_1 = 0$ else; $q_2 = 2$ if $\mathcal{E}_i^R \cap \mathcal{P}_k \neq \emptyset$, $q_2 = 0$ else; and $q_3 = 3$ if $\mathcal{E}_i^L \cap \mathcal{P}_k \neq \emptyset$, $q_3 = 0$ else.

Remark 2. *In the case where the plane is considered perfectly safe for the tether without risk of snagging or clipping, the Theorem 6 can be adapted such that $\mathcal{S}_i \cap \mathcal{P}_k = \emptyset$ only if $\left(\mathcal{E}_i^R \cap \mathcal{P}_k = \emptyset\right) | \left(\mathcal{E}_i^O \cap \mathcal{P}_k = \emptyset\right)$ and $q_3 = 0$ in all cases.*

The Theorem 11 in Appendix A.2 provides a test to know if a plane $\mathcal{P}_k$ and an ellipsoid $\mathcal{E}_i$ intersect, *i.e.* if $\mathcal{E}_i \cap \mathcal{P}_k \neq \emptyset$.

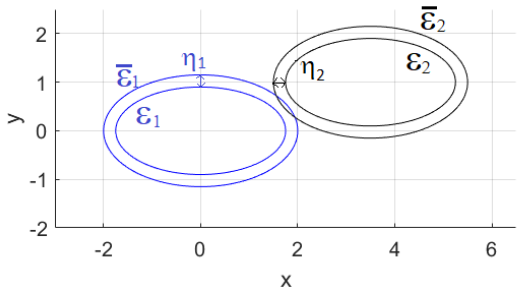

Figure 7: Two examples of two ellipsoids $\mathcal{E}_1$ and $\mathcal{E}_2$ and their layers $\bar{\mathcal{E}}_1$ and $\bar{\mathcal{E}}_2$.

5.5. Prediction collision: ellipsoid layer

To perform an obstacle avoidance, the obstacle must be detected before the collision occurs. Thus, we propose to envelop the ellipsoids in a larger one, called a "layer", to detect potential future collisions. If an intersection occurs between two layers, an obstacle avoidance procedure is triggered.

The following definition describes the chosen layer shape.

Definition 6. *For a chosen thickness $\eta_i \geq 0$, let define $\bar{\mathcal{E}}_i(\eta_i)$ the layer of ellipsoid $\mathcal{E}_i$ such that $\bar{\mathcal{E}}_i(\eta_i)$ is an ellipsoid as defined in Definition 1 with the parameters $\bar{a}_i = a_i + \eta_i$, $\bar{b}_i = b_i + \eta_i$, $\bar{c}_i = c_i + \eta_i$ and $\bar{C}_i = C_i$ where a_i, b_i, c_i and C_i are the parameters of $\mathcal{E}_i$. Moreover, since all axis of $\bar{\mathcal{E}}_i(\eta_i)$ are larger that those of $\mathcal{E}_i$ and both as the same center, one has $\mathcal{E}_i \subseteq \bar{\mathcal{E}}_i(\eta_i)$ and $\bar{\mathcal{E}}_i(0) = \mathcal{E}_i$.*

By extension, let define $\bar{\mathcal{S}}_i(\eta_i^L, \eta_i^R, \eta_i^O)$ $= \{\bar{\mathcal{E}}_i^L(\eta_i^L), \bar{\mathcal{E}}_i^R(\eta_i^R), \bar{\mathcal{E}}_i^O(\eta_i^O)\}$ the layer of the system $\mathcal{S}_i = \{\mathcal{E}_i^L, \mathcal{E}_i^R, \mathcal{E}_i^O\}$, where $\eta_i^L \geq 0$, $\eta_i^R \geq 0$ and $\eta_i^O \geq 0$.

The layer $\bar{\mathcal{E}}_i(\eta_i)$ of $\mathcal{E}_i$ is illustrated in Figure 7. The formalist exposed in Definition 6 has been chosen because it has observed in practice that, for each point on the surface $\mathcal{E}_i$, the distance to the nearest point of $\bar{\mathcal{E}}_i$ is equal to η_i. However, as we have not found a proof of this property, it won't be used in this document.

Choice of the layer thickness η_i The main difficult of $\bar{\mathcal{E}}_i(\eta_i)$ is to choose the thickness η_i. Since the aim of the layer is to predict collision, we propose to choose η_i such that for two instants $0 < t_k < t_{k+1}$, the shape of ellipsoid $\mathcal{E}_i(t_{k+1})$ is still inside its previous layer ellipsoid $\bar{\mathcal{E}}_i(\eta_i, t_k)$, *i.e.* $\mathcal{E}_i(t_{k+1}) \subseteq \bar{\mathcal{E}}_i(\eta_i, t_k)$. Thus, if no other obstacle are in contact with $\bar{\mathcal{E}}_i$, there is no risk of collision, see Theorem 7.

Theorem 7. *For $\ell \in \{i, j\}$, let define $\mathcal{E}_\ell(t_k)$ and $\bar{\mathcal{E}}_\ell(\eta_\ell, t_k)$ an ellipsoid and its layer at an instant $t_k > 0$. For $t \in [t_k, t_{k+1}]$ with $t_{k+1} > t_k$, suppose that $\forall \ell \in \{i, j\}$, $\mathcal{E}_\ell(t) \subseteq \bar{\mathcal{E}}_\ell(\eta_\ell, t_k)$. Thus, if there is not intersection between layers $\bar{\mathcal{E}}_i(\eta_i, t_k)$ and $\bar{\mathcal{E}}_j(\eta_j, t_k)$, i.e. $\bar{\mathcal{E}}_i(\eta_i, t_k) \cap \bar{\mathcal{E}}_j(\eta_j, t_k) = \emptyset$, then there is not risk of collision between $\mathcal{E}_i(t)$ and $\mathcal{E}_j(t)$, i.e. $\mathcal{E}_i(t) \cap \mathcal{E}_j(t) = \emptyset$ for $t \in [t_k, t_{k+1}]$. Else, a risk of collision is possible.*

Same comments can be made between
(1)$\mathcal{S}_i(t_k)$ and $\mathcal{S}_j(t_k)$ using $\bar{\mathcal{S}}_\ell(\eta_\ell^L, \eta_\ell^R, \eta_\ell^O, t_k)$ with $\ell \in \{i, j\}$;
(2)$\mathcal{E}_i(t_k)$ and $\mathcal{S}_j(t_k)$ using $\bar{\mathcal{S}}_i(\eta_i^L, \eta_i^R, \eta_i^O, t_k)$ and $\bar{\mathcal{E}}_j(t_k)$;
(3)$\mathcal{E}_i(t_k)$ and a plane $\mathcal{P}_k$ using $\bar{\mathcal{E}}_i(t_k)$ and $\mathcal{P}_k$.
and so Theorems 2, 3, 4 and 6 using the layer notation.

The proof of Theorem 7 is in the theorem itself. In the same way, we can define $\bar{\mathcal{L}}_{\text{obs}}^i$ and $\bar{\mathcal{L}}_Q^i$the list of obstacle layers of the system $\mathcal{S}_i$.

Since the tether i shape changes when ROV R_i moves, it is not trivial to how to choose η_i such that $\mathcal{E}_i(t_{k+1}) \subseteq \bar{\mathcal{E}}_i(\eta_i, t_k)$ $\forall t \in [t_k, t_{k+1}]$. We proposed here to arbitrary choose η_i based on observations, then constrain the ROV's displacement such that the tether gets out of its layer. This displacement is limited using α_{R_i}, as exposed in Section 8.2. Note that the faster you want an ROV to move, the larger the layer must be.

Note that $\eta = 0$ is a valid solution for an immobile obstacle. In practice, depending on how dangerous the obstacle is (mine, sharp-edged obstacle, etc.), an additional safety distance inducing $\eta > 0$ can be chosen: this comment will be more developed in Section 9.

Remark 3. *Since $\mathcal{E}_i^L(t_{k+1})$ and $\bar{\mathcal{E}}_i^L(\eta_i, t_k)$ share the focal point O_i, $\mathcal{E}_i^L(t_{k+1}) \subseteq \bar{\mathcal{E}}_i^L(\eta_i, t_k) \Leftrightarrow \mathcal{E}_i^L(t_{k+1}) \cap \bar{\mathcal{E}}_i^L(\eta_i, t_k) = \emptyset$.*

6. Obstacle avoidance

To avoid a collision with an obstacle $\mathcal{A}_j^i$, three strategies are used based on Q_{ij}:

- **Repelling strategy** to move the ROV away from the obstacle if $Q_{ij} \in \{2, 3\}$, based on APF;
- **Anti-crossing collision** to untie the knot if $Q_{ij} = 4$;
- **Reduction of tether's length** to reduce the size of the ellipsoid if $Q_{ij} = 3$.

The impact of these strategies on the ROV motion is described in Section 6.4, and a strategy to bypass more efficiently some obstacle is described in Section 7.3. One can observe that no strategy is used if $Q_{ij} = 0$ or $Q_{ij} = 1$. Indeed, $Q_{ij} = 0$ means there is no collision, and $Q_{ij} = 1$ corresponds to the case where $\mathcal{E}_i^O$ is in collision, *i.e.* the anchor O_i. However, since O_i is supposed to be fixed (Assumption A2), the system $\mathcal{S}_i$ is unable to resolve this collision: only obstacle $\mathcal{A}_j^i$ can.

Remind the collisions are detected using the layers $\bar{\mathcal{S}}_i$ and $\bar{\mathcal{A}}_j^i$, but notations $\mathcal{S}_i$ and $\mathcal{A}_j^i$ will be used by comfort in the rest of the paper.

6.1. Repelling strategy

Let $\hat{R}_i^*(t)$ be the current target followed by ROV R_i at instant t, as it will be defined in Section 7.3.2. When a collision of type $Q_{ij} \in \{2, 3\}$ is detected between $\mathcal{S}_i$ and an obstacle $\mathcal{A}_j^i$, a repulsive force noted $\vec{f}_r^{i,j}$ is applied on the ROV i to move away from $\mathcal{A}_j^i$.

6.1.1. Repelling from a plane

If $\mathcal{A}_j^i$ is a plane, *i.e.* $\mathcal{A}_j^i \in \mathcal{L}_\mathcal{P}$ and $\mathcal{A}_j^i = \mathcal{P}_j\left(P_j, \vec{n}_j\right)$, then the repulsion follows the normal to the plane $\vec{n}_j$ such that $\vec{f}_r^{i,j} = \frac{\vec{n}_j}{\|\vec{n}_j\|}$.

6.1.2. Repelling from an ellipsoid full-obstacle $\mathcal{E}_j$

If $\mathcal{A}_j^i \in \mathcal{L}_\mathcal{O}^i$, let's name $\mathcal{E}_j$ the ellipsoid obstacle such as $\mathcal{E}_j = \mathcal{A}_j^i$. The ROV i is repulsed from $\mathcal{E}_j$ following the three following potential field: one repulsive force $\vec{v}_1$ from the main axis and the extremities of the ellipsoid, and two "rotary" forces $\vec{v}_2$ and $\vec{v}_3$ to help to bypass the obstacle in direction of the objective $\hat{R}_i^*$, as illustrated in Figure 8. These three forces are combined to give global repulsive force $\vec{f}_r^{i,j}$.

Definition 7. *Let's define the notation* $\|.\|_u$ *such that* $\forall \vec{x} \in \mathbb{R}^3$,

$$\|\vec{x}\|_u = \begin{cases} \|\vec{x}\| & \text{if } \|\vec{x}\| \neq 0, \\ 1 & \text{else.} \end{cases} \tag{19}$$

For the system $\mathcal{S}_i$ and an ellipsoid obstacle $\mathcal{E}_j$, the global repulsive force $\vec{f}_r^{i,j}$ can be expressed as

$$\vec{f}_r^{i,j}\left(\mathcal{E}_j\right) = \frac{2\vec{v}_1 + \vec{v}_2 + \vec{v}_3}{\|2\vec{v}_1 + \vec{v}_2 + \vec{v}_3\|_u} \tag{20}$$

where $\vec{v}_1$, $\vec{v}_2$ and $\vec{v}_3$ can be expressed as

$$\vec{v}_1 = \frac{\vec{\bar{v}}_1}{\left\|\vec{\bar{v}}_1\right\|_u} \tag{21}$$

$$\vec{v}_2 = \frac{\vec{v}_{20}}{\|\vec{v}_{20}\|_u}\text{sign}\left(\vec{v}_{20}.\vec{v}_{\text{rot2}}\right) \tag{22}$$

$$\vec{v}_3 = \frac{\vec{v}_{30}}{\|\vec{v}_{30}\|_u}\text{sign}\left(\vec{v}_{30}.\vec{v}_{\text{rot3}}\right) \tag{23}$$

where

$$\vec{\bar{v}}_1 = \begin{cases} \vec{F_{1,j}R_i} & \text{if } \left(\left|\vec{v}_{d_j}.\vec{F_{2,j}R_i}\right| > d_j\right) \\ & \quad \& \left(\left\|R_iF_{1,j}\right\| < \left\|R_iF_{2,j}\right\|\right) \\ \vec{F_{2,j}R_i} & \text{if } \left(\left|\vec{v}_{d_j}.\vec{F_{1,j}R_i}\right| > d_j\right) \\ & \quad \& \left(\left\|R_iF_{1,j}\right\| > \left\|R_iF_{2,j}\right\|\right) \\ \vec{v}_{10} & \text{else.} \end{cases} \tag{24}$$

with $\vec{v}_{10} = \vec{C_jR_i} - \vec{v}_{d_j}\left(\vec{v}_{d_j}.\vec{C_jR_i}\right)$, $\vec{v}_{d_j} = \frac{\vec{d}_j}{\|\vec{d}_j\|}$ and

$$\vec{v}_{20} = \vec{v}_1 \wedge \vec{v}_{30} \tag{25}$$

$$\vec{v}_{30} = \vec{v}_1 \wedge \vec{v}_{d_j} \tag{26}$$

$$\vec{v}_{\text{rot2}} = \left(\vec{v}_0 \wedge \vec{v}_{30}\right)\text{sign}\left(\left(\vec{v}_0 \wedge \vec{v}_{30}\right).\vec{v}_4\right) \tag{27}$$

$$\vec{v}_{\text{rot3}} = \left(\vec{v}_0 \wedge \vec{v}_{d_j}\right)\text{sign}\left(\left(\vec{v}_0 \wedge \vec{v}_{d_j}\right).\vec{v}_4\right) \tag{28}$$

where $\vec{v}_0 = \vec{C_jR_i}$ and $\vec{v}_4 = \vec{R_i\hat{R}_i^*}$.

Detail of previous calculation is detailed in Appendix B.7.

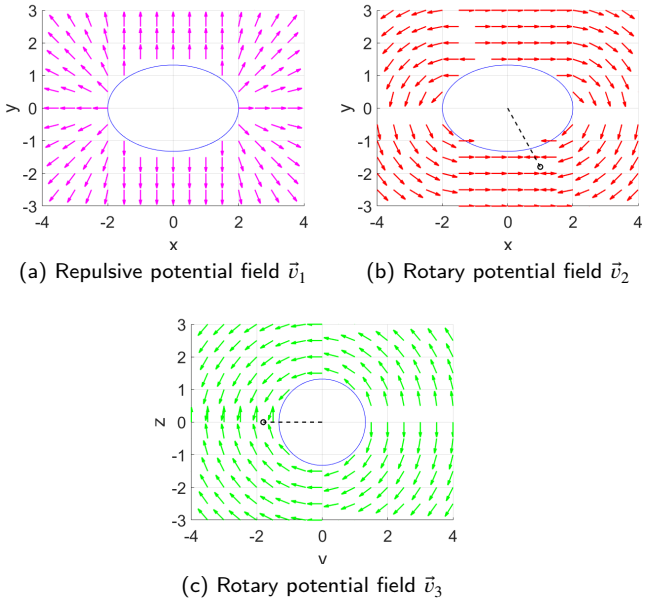

(a) Repulsive potential field $\vec{v}_1$ (b) Rotary potential field $\vec{v}_2$

(c) Rotary potential field $\vec{v}_3$

Figure 8: Representation of repulsive potential fields $\vec{v}_1$, $\vec{v}_2$ and $\vec{v}_3$ in $\mathcal{R}_{\mathcal{E}_j}$. Small black circle: target $\hat{R}_i^*$. Dash line: $\left[C_j\hat{R}_i^*\right]$. $\vec{v}_1$ pushes always the ROV to $\mathcal{E}_j$. $\vec{v}_2$ and $\vec{v}_3$helps to bypass $\mathcal{E}_j$ in direction of the objective.

Remark 4. *The first idea to create* $\vec{v}_1$ *was to use the Jacobian matrix of* $\mathcal{E}_j$*, but it was more difficult for the ROV to go around* $\mathcal{E}_j$ *near its extremities when* $\mathcal{E}_j$ *is flat. See more details in Appendix B.7.*

6.1.3. Repelling from an tether obstacle system $\mathcal{S}_j$

In case of a system obstacle $\mathcal{S}_j$, *i.e.* $\mathcal{A}_j^i \in \mathcal{L}_\mathcal{S}^{(-i)}$, three ellipsoids can be involved. Let $\vec{v}_1\left(\mathcal{S}_j\right)$ be the evaluation of $\vec{\bar{v}}_1$ as exposed in Section 6.1.2 using parameter of ellipsoid $\mathcal{E}_j^L$, similarly for $\mathcal{E}_j^O$ and $\mathcal{E}_j^R$ and for the evaluation of $\vec{v}_2\left(\mathcal{E}_j^L\right)$ and $\vec{v}_3\left(\mathcal{E}_j^L\right)$.

Go around $\mathcal{S}_j$ is more complex. Indeed, $\vec{v}_2$ and $\vec{v}_3$ will push in most case the ROV R_i at the intersection between $\mathcal{E}_j^L$ and $\mathcal{E}_j^O$ or $\mathcal{E}_j^R$, even more so if they are summed for the three ellipsoids. Since $\mathcal{E}_j^L$ is the center of the system $\mathcal{S}_j$, the proposed solution is to consider the global repulsive force $\vec{f}_r^{i,j}\left(\mathcal{E}_j^L\right)$ in all case and add the repulsive forces $\vec{v}_1\left(\mathcal{E}_j^O\right)$ and $\vec{v}_1\left(\mathcal{E}_j^R\right)$ to avoid collision with $\mathcal{E}_j^O$ and $\mathcal{E}_j^R$ when going around them:

$$\vec{f}_r^{i,j}\left(\mathcal{S}_j\right) = \frac{2\vec{v}_1\left(\mathcal{S}_j\right) + \vec{v}_2\left(\mathcal{E}_j^L\right) + \vec{v}_3\left(\mathcal{E}_j^L\right)}{\left\|2\vec{v}_1\left(\mathcal{S}_j\right) + \vec{v}_2\left(\mathcal{E}_j^L\right) + \vec{v}_3\left(\mathcal{E}_j^L\right)\right\|_u} \tag{29}$$

where $\vec{v}_2\left(\mathcal{E}_j^L\right)$ and $\vec{v}_3\left(\mathcal{E}_j^L\right)$ are evaluated using (22) and (23) and $\vec{v}_1\left(\mathcal{S}_j\right) = \frac{\vec{v}_1(\mathcal{S}_j)}{\left\|\vec{v}_1(\mathcal{S}_j)\right\|_u}$ where

$$\vec{v}_1\left(\mathcal{S}_i\right) = \vec{v}_1\left(\mathcal{E}_j^L\right) + \vec{v}_1\left(\mathcal{E}_j^O\right) q_O^{i,j} + \vec{v}_1\left(\mathcal{E}_j^R\right) q_R^{i,j} \tag{30}$$

where $\vec{v}_1(.)$ is evaluated using (21), $q_O^{i,j} = 1$ if $\mathcal{S}_i \cap \mathcal{E}_j^O \neq 0$ ($\Leftrightarrow Q_{ji} = 1$), $q_O^{i,j} = 0$ else and $q_R^{i,j} = 1$ if $\mathcal{S}_i \cap \mathcal{E}_j^R \neq 0$ ($\Leftrightarrow Q_{ji} = 2$), $q_R^{i,j} = 0$ else.

6.2. Anti-crossing collision

When a crossing collision as defined in Theorem 5 is detected with an obstacle $\mathcal{A}_j^i \in \mathcal{L}_S^{(-i)}$, *i.e.* $Q_{ij} = 4$, the ROV must go back to undo the knot that is forming. A displacement following the vector $\vec{f}_a^{i,j}$ is performed, with

$$\vec{f}_a^{i,j} = \frac{\bar{S}_i\bar{S}_j}{\left\|\vec{\bar{S}_i\bar{S}_j}\right\|_u} \tag{31}$$

where $\bar{S}_i$ and $\bar{S}_j$ the closest points between $\mathcal{E}_i^L(t)$ and $\mathcal{E}_j^L(t)$ of system $\mathcal{S}_i$ and $\mathcal{S}_j = \mathcal{A}_j^i$. Remind $\bar{S}_i(t)$ and $\bar{S}_j(t)$ can be evaluated using Theorem 10 in Appendix A.1.

6.3. Tether length reduction

When the tether is in collision with an obstacle $\mathcal{A}_j^i$, *i.e.* $Q_{ij} = 3$, this may be due to the cable being too loose between O_i and R_i. A solution can be to reduce the length L_i to reduce the volume of $\mathcal{E}_i^L$ and so avoid the collision. Note that L_i could be reduce until it becomes a line, but underwater navigation with a stretched cable between it and its reel is not simple, that's why we prefer in most cases to keep the tether a minimum loosen.

If $\exists Q_{ij} \in \mathcal{L}_Q^i$ such that $Q_{ij} = 3$, L_i is reduced so that $L_i\left(t_{k+1}\right) = L_i\left(t_k\right) - \delta L_{\max}$ if $\left(L_i\left(t_k\right) - \delta L_{\max}\right) < d_{\text{next}}\left(t_k\right)$ with $d_{\text{next}}\left(t_k\right) = \left\|O_iR_i\right\|\left(t_k\right) + V_{R_i\max}\Delta T$, else the ROV could be blocked by the cable in its next move. Note that since L_i is not reduced when there is no collision, some additional optional rules could be added to avoid the tether to become too long and so generate too much drag force, for example reduce L_i if $L_i > 2\left\|O_iR_i\right\|\left(t_k\right)$.

6.4. Multi-collision management

Previous sections exposed repulsive forces to avoid an single obstacle. The combination of these forces for several obstacle provides a target motion vector $\vec{v}_{R_i}$, as described by the following Algorithm 1.

To limit local minima inherent to potential field method, we add in the algorithm the following test: if the found vector $\vec{v}_{R_i}$ points in the direction opposite to the ROV's target (we choose $180° \pm 10°$ here), then we add a random component $\vec{u}_{\text{rand }3\times1} \in \mathbb{R}^3$ to try to escape the local minimum.

Algorithm 1 Mutli-collision avoidance

Require: $\hat{R}_i^*$, $\mathcal{L}_Q^i$
Need_Reduction_L = False
$\vec{v}_{R_i} = \begin{bmatrix} 0 & 0 & 0 \end{bmatrix}^T$
for j in $1 : N_{\text{obs}}$ **do**
  if $Q_{ij} = 4$ **then**
    Anti-crossing collision strategy: $\vec{v}_{Q_{ij}} = 3\vec{f}_a^{i,j}$
  else if $Q_{ij} = 3$ **then**
    Repelling strategy: $\vec{v}_{Q_{ij}} = \vec{f}_r^{i,j}$,
    Need_Reduction_L = True
  else if $Q_{ij} = 2$ **then**
    Repelling strategy: $\vec{v}_{Q_{ij}} = \vec{f}_r^{i,j}$
  else
    $\vec{v}_{Q_{ij}} = \begin{bmatrix} 0 & 0 & 0 \end{bmatrix}^T$
  end if
  $\vec{v}_{R_i} = \vec{v}_{R_i} + \vec{v}_{Q_{ij}}$
end for
$\vec{v}_{R_i} = \frac{\vec{v}_{R_i}^*}{\left\|\vec{v}_{R_i}\right\|_u}$
if $\left(\vec{v}_{R_i} \cdot \frac{\vec{R_iR_i^*}}{\left\|\vec{R_iR_i}\right\|_u}\right) < \cos(170°)$ **then**
  $\vec{v}_{R_i} = \vec{v}_{R_i}^* + 0.1\vec{u}_{\text{rand }3\times1}$ % add random unit vector
  $\vec{v}_{R_i} = \frac{\vec{v}_{R_i}}{\left\|\vec{v}_{R_i}\right\|_u}$
end if
% Reduction of L_i if need
if Need_Reduction_L = True **then**
  if $\left(L_i\left(t_k\right) - \delta L_{\max}\right) < \left\|O_iR_i\right\|\left(t_k\right) + V_{R_i\max}\Delta T$ **then**
    $L_i = L_i - \delta L_{\max}$
  end if
end if
return $\vec{v}_{R_i}$, L_i, Need_Reduction_L

7. Path to the target objective

7.1. Hypotheses on the target

Let R_i^* be the final target of R_i. Since underwater obstacles are often sharp and so the possibility of making a bend in the cable is excluded, the target R_i^* of ROV R_i is reachable only if

- the tether is long enough to reach the target, *i.e.* $\left\|O_iR_i^*\right\| < L_{i,\max}$;
- there exist a line $O_iR_i^*$ free of full-obstacles $\mathcal{O}_m$ on it, *i.e.* $\exists L_i \in \left[0, L_{i,\max}\right]$ such that $\mathcal{S}_i \cap \mathcal{O}_m = \emptyset$ $\forall m \in [1 \dots M]$ when $R_i = R_i^*$;
- $\forall (i,j) \in \mathcal{N}^2$, each target R_i^* has been chosen such that there is no collision between their layers when all targets have been reached, *i.e.* $\forall i \in \mathcal{N}$ one has $\bar{S}_i \cap \bar{S}_j = \emptyset$ (following Theorem 4) when $R_i = R_i^*$. It can induce to reduce the layer η_i when ROV i

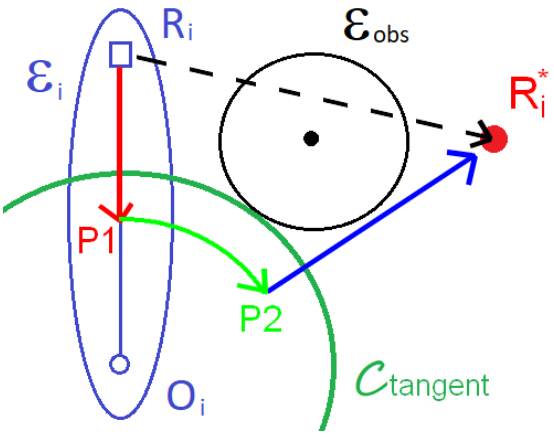

Figure 9: Bypass strategy: following the colored arrows, the ROV R_i can avoid the collision between its tether and the obstacle $\mathcal{E}_{\text{obs}}$. Repulsive strategy is used in parallel to avoid collision. Blue ellipsoid: $\mathcal{E}_i$. Red circle: target to reach. Black circle: obstacle $\mathcal{E}_{\text{obs}}$. Green circle: circles tangent to $\mathcal{E}_{\text{obs}}$ with center O_i. Black dotted line: shortest path. $P1$ and $P2$: intermediate targets. $\mathcal{C}_{\text{tangent}}$ is the circle tangent to $\mathcal{E}_{\text{obs}}$ and center in O_i.

has reached its target (for example take $\eta_i = 0$ when $R_i = R_i^*$).

In an ideal configuration, the shortest path between R_i and R_i^* would be the direct line $R_iR_i^*$, as illustrated by the black dash line in Figure 9. However, the presence of an obstacle on the path can induce to bypass it, as exposed in next section and illustrated by colored lines in Figure 9.

7.2. Detection of obstacles on the path

The avoidance strategies presented in Section 6 can lead to bypassing the obstacle while avoiding it, but it is more efficient to anticipate and choose another path when an obstacle is detected on the way, as illustrated in Figure 9.

As planes are assumed to be infinite in this study and so cannot be bypassed, only ellipsoidal obstacles are considered here.

Definition 8. *For a system $\mathcal{S}_i$, an ellipsoid $\mathcal{E}_{obs}$ is considered on the path between R_i and its target R_i^* if the main axis $d_i = [F_{1,i}F_{2,i}] = [O_iR_i]$ of $\mathcal{E}_i^L$ will have to intersect with $d_{obs} = [F_{1,obs}F_{2,obs}]$ to reach R_i^*, i.e. the intersection between d_{obs} and triangle $O_iR_iR_i^*$ is not empty, i.e. $d_{obs} \cap O_iR_iR_i^* \neq \emptyset$. Systems obstacle $\mathcal{S}_j$ are considered as three different and independent ellipsoidal obstacles $\mathcal{E}_{obs}$.*

The Figure 10 illustrates the intersection between $\mathcal{E}_{obs}$ and the triangle $O_iR_iR_i^*$.

The Theorem 12 in Appendix A.3 provides a method to check the conditions of Definition 8. Since there may be several obstacles between R_i and R_i^*, we define $\mathcal{L}^i_{\mathcal{O}\text{bypass}}(t) = \left\{\mathcal{E}^{i,1}_{\text{obs}}, \dots, \mathcal{E}^{i,J}_{\text{obs}}\right\}$ the list of obstacles on the path between R_i and its target R_i^* at an instant t with $J > 0$ the number of element of $\mathcal{L}^i_{\mathcal{O}\text{bypass}}(t)$. Note that J changes with time and/or position of R_i.

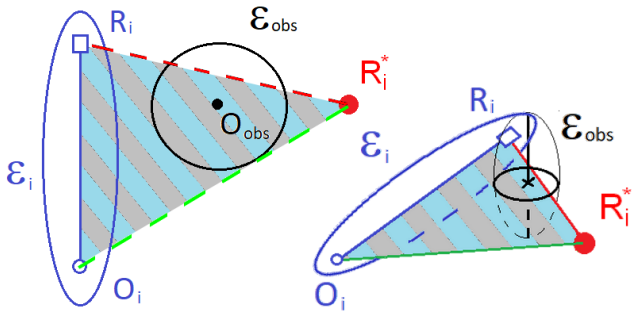

Figure 10: Intersection between the triangle $O_iR_iR_i^*$ and the ellipsoid obstacle $\mathcal{E}_i$.

7.3. Bypass strategy

When at least one obstacle between R_i and R_i^* is detected, *i.e.* $\mathcal{L}^i_{\mathcal{O}\text{bypass}}(t) \neq \emptyset$, the bypass strategy is applied. The bypass strategy is divided in three steps, illustrated in Figure 9:

1. Folding the system $\mathcal{S}_i$ inside a folding circle area $\mathcal{C}^i_{\text{bypass}}\left(O_i, r^i_{\text{bypass}}\right)$ of center O_i and radius r^i_{bypass};
2. Go around the obstacle staying inside $\mathcal{C}^i_{\text{bypass}}$;
3. Go towards the target R_i^* once the obstacle has been bypassed, *i.e.* when $\mathcal{L}^i_{\mathcal{O}\text{bypass}}(t) = \emptyset$.

The choice of the folding area $\mathcal{C}^i_{\text{bypass}}$ is described in Section 7.3.1. To perform the bypass strategy, the ROV will follow sub-targets $\hat{R}_i^*(t)$, where $\hat{R}_i^*(t) = R_i^*$ if $\mathcal{L}^i_{\mathcal{O}\text{bypass}}(t) = \emptyset$. These sub-target are described in Section 7.3.2.

7.3.1. Definition of bypass circle $\mathcal{C}^i_{bypass}$

For each obstacle $\mathcal{E}^{i,j}_{\text{obs}} \in \mathcal{L}^i_{\mathcal{O}\text{bypass}}(t)$, we can define a circle $\mathcal{C}^{i,j}_{\text{tangent}}\left(\mathcal{E}^{i,j}_{\text{obs}}, O_i, r^{i,j}_{\text{tangent}}\right)$ tangent to $\mathcal{E}^{i,j}_{\text{obs}}$, centered in O_i and with a radius $r^{i,j}_{\text{tangent}}$, as illustrated in green in Figure 9. The Theorem 13 in Appendix A.4 proposes a method to evaluate $\mathcal{C}^{i,j}_{\text{tangent}}$.

Since the system $\mathcal{S}_i$ (ROV+tether+anchor) stay inside $\mathcal{C}^i_{\text{tangent}}$, there is no risk of collision between $\mathcal{S}_i$ and $\mathcal{E}^{i,j}_{\text{obs}}$. Note that depending of the tether length L_i, $\mathcal{E}_i^L$ may be too big to fit inside $\mathcal{C}^{i,j}_{\text{tangent}}$ even when $R_i = O_i$: a reduction of the length L_i may be required to avoid collision. Remark also that the smallest circle in which $\mathcal{S}_i$ can be contained is a circle of center O_i and radius $r_{\min,i} = a_i^O + 2a_i^R$ where a_i^O and a_i^R are the semi-main axis of $\mathcal{E}_i^O$ and $\mathcal{E}_i^R$. Thus, we will chose $r^i_{\text{bypass}} \geq r_{\min,i}$ as minimum even if $r_{\min,i} > r^{i,j}_{\text{tangent}}$. In this case, the second part of the bypass will be managed by the repelling strategy presented in Section 6.1.

Then, r^i_{bypass} can be expressed as

$$r^i_{\text{bypass}} = \max\left(\left[a_i^O + 2a_i^R, r^i_{\text{tangent}}\right]\right) \tag{32}$$

with a_i^O and a_i^R are the semi-main axis of $\mathcal{E}_i^O$ and $\mathcal{E}_i^R$ and

$$r^i_{\text{tangent}} = \min\left(\mathcal{L}^i_{r,\text{tangent}}\right) \tag{33}$$

where $\mathcal{L}^i_{r,\text{tangent}} = \left\{ r^{i,j}_{\text{tangent}} \mid j \in \left[1 \dots N_{\text{obs}}\right], \mathcal{A}^i_j \in \mathcal{L}^i_{\mathcal{O}\text{bypass}}(t) \right\}$ the list of radius $r^{i,j}_{\text{tangent}}$ associated to the obstacles on the path of $\mathcal{S}_i$.

7.3.2. *Choice of target* $\hat{R}^*_i(t)$

Based on previous sections and to perform the bypass strategy if require, the sub-target $\hat{R}^*_i(t)$ can be expressed as

$$\hat{R}^*_i(t) = \begin{cases} P^i_1(t) & \text{if } \left(\left\|O_iR_i\right\| > r^i_{\text{bypass}}(t)\right) \\ & \quad \& \left(\mathcal{L}^i_{\mathcal{O}\text{bypass}}(t) \neq \emptyset\right) \\ P^i_2(t) & \text{if } \left(\left\|O_iR_i\right\| < r^i_{\text{bypass}}(t)\right) \\ & \quad \& \left(\mathcal{L}^i_{\mathcal{O}\text{bypass}}(t) \neq \emptyset\right) \\ R^*_i & \text{else} \end{cases} \tag{34}$$

where

$$P^i_1(t) = O_i + \frac{\vec{O_iR_i}}{\left\|O_iR_i\right\|}\left(r^i_{\text{bypass}}(t) - \frac{d^R_i}{2}\right) \tag{35}$$

$$P^i_2(t) = O_i + \frac{\vec{O_iR^*_i}}{\left\|O_iR^*_i\right\|}\left(r^i_{\text{bypass}}(t) - \frac{d^R_i}{2}\right) \tag{36}$$

Note that the sub-target $P^i_1(t)$ depends of the current ROV position and so is adjustable with the eventual perturbations due to the obstacle avoidance strategies.

The choice of $\hat{R}^*_i(t)$ and the bypass strategy is summarized in Algorithm 6 in Appendix A.5.

8. ROV motion

Based on methods exposed in previous sections, Algorithm 2 exposes how to choose $\vec{v}_{R_i}(t_k)$ and $\alpha_{R_i}(t_k)$ such that the ROV motion to reach its next position. One observes that the proposed solution is distributed because it can be evaluated by each ROV independently and does not consider the decision of others ROVs or moving obstacles to choose its trajectory.

When a ROV i reaches its objective, it maintains its position and thus is considered as immobile, *i.e.* one takes $\alpha_{R_i} = 0$, but it can still adjust its umbilical length L_i.

For the ROV reaches its next position $R_i(t_{k+1})$, the tether L_i may need to be extended. The tether extension is described in Section 8.1. In parallel, to guarantee that the condition $\mathcal{S}_i(t_{k+1}) \not\subseteq \bar{\mathcal{S}}_i(\eta_i, t_k)$ introduced in Section 5.5 to prevent collisions is respected, two solutions are proposed: reduce the length L_i if possible (see Section 6.3), or limit the velocity α_{R_i} (see in Section 8.2). The combination of tether management and velocity limitation is described in Algorithm 4.

Algorithm 2 ROV motion

Require: R^*_i, $L_i(t_k)$

1: Estimate current target: Algorithm 6→ $\hat{R}^*_i$
2: For $\mathcal{A}^i_j \in \mathcal{L}^i_{\text{obs}}$, estimation of potential collision using layer $\bar{\mathcal{S}}_i$ and $\bar{\mathcal{A}}^i_j \rightarrow \mathcal{L}^i_{\mathcal{Q}}$
3: **if** $\max\{\mathcal{L}^i_{\mathcal{Q}}\} = 0$, *i.e.* there is no risk of collision **then**
4: $\quad \vec{v}_{R_i} = \frac{\vec{R_iR^*_i}}{\left\|\vec{R_iR^*_i}\right\|}$
5: $\quad$ Need_Reduction_L $= False$
6: **else**
7: $\quad$ Obstacle avoidance Algorithm 1 → $\vec{v}_{R_i}$, L_i, Need_Reduction_L
8: **end if**
9: **if** $\left\|R_iR^*_i\right\| < \varepsilon_i$ **then**
10: $\quad \alpha_{R_i} = 0$ % The target is reached
11: **else**
12: $\quad$ % Choice of α_{R_i} and L_i to guarantee $\mathcal{S}_i(t) \subseteq \bar{\mathcal{S}}_i(\eta_i, t_k)$ using Algorithm 4 → $\alpha_{R_i}(t_{k+1})$, $L_i(t_{k+1})$
13: **end if**
14: $R_i(t_{k+1})$ using (16) with $\vec{v}_{R_i}(t_{k+1})$, $\alpha_{R_i}(t_{k+1})$ % New position
15: **return** $\vec{v}_{R_i}(t_{k+1})$, $\alpha_{R_i}(t_{k+1})$ and $L_i(t_{k+1})$

8.1. Tether length extension

When the estimate position $\hat{R}_i(t_k, \alpha^*_i, \vec{v}_i)$ cannot be reached in practice due to the tether length L_i, this one can be extended such that

$$L_i(t_{k+1}) = \min\left\{L_i(t_k) + \Delta L, L_{i,\max}\right\} \tag{37}$$

with $\Delta L = \min\left(\left[V_{R_i\max}\Delta T,\ \delta L_{\max}\right]\right)$ the maximum roll-out. L_i is extended iff

- $L_i(t_k) < \left\|O_i\hat{R}_i(t_k, \alpha^*_i, \vec{v}_i)\right\|$, *i.e.* the tether is too short to reach the next position, where $(\alpha^*_i, \vec{v}_i)$ are defined in Algorithm 1;
- $L_i(t_{k+1}) < \min\left\{\left\|O_iR^*_i\right\| + \delta_L, L_{i,\max}\right\}$ with $\delta_L > 0$ a chosen parameter, *i.e.* the cable is not extended any further than is necessary to reach its target (or its maximal length) since bends in the cable are very limited in this study. ;
- L_i has not been reduced during time interval $[t_k,\ t_{k+1}]$;
- the new length $L_i(t_{k+1})$ does not lead to $\mathcal{E}^L_i(t_{k+1}) \not\subseteq \bar{\mathcal{E}}^L_i(\eta_i, t_k)$.

In the case where $L_i(t_{k+1})$ is still too short to reach $\hat{R}_i(t_k, \alpha^*_i, \vec{v}_i)$ (or cannot be extend), the target position is readjusted to obtain a reachable one:

$$\hat{R}_i = \frac{L_i(t_{k+1})}{\left\|O_i\hat{R}^*_i\right\|}\vec{O_i\hat{R}_i} + O_i. \tag{38}$$

These rules are summarized in Algorithm 3.

Algorithm 3 Extend L_i

Require: $L_i\left(t_k\right)$, $\hat{R}_i$, Need_Reduction_L
$\tilde{L}_i = L_i$
if $L_i\left(t_k\right) < \left\|O_i\hat{R}_i\right\|$ **then**
  % The target is unreachable because L_i too short
  if $\left(L_i\left(t_k\right) < \min\left\{\left\|O_iR_i^*\right\| + \delta_L, L_{i,\max}\right\}\right)$ &(Need_Reduction_L = False) **then**
    % It is possible to extend L_i
    $\tilde{L}_i = \min\left\{L_i\left(t_k\right) + \Delta L, L_{i,\max}\right\}$ with $\Delta L = \min\left(\left[V_{R_i\max}\Delta T,\ \delta L_{\max}\right]\right)$
  end if
  % If $\tilde{L}_i$ still too short, the estimate position is readjusted
  if $\tilde{L}_i < \left\|O_i\hat{R}_i\right\|$ **then**
    $\hat{R}_i = \frac{\tilde{L}_i}{\left\|O_i\hat{R}_i^*\right\|}\vec{O_i\hat{R}_i} + O_i$
  end if
end if
return $\tilde{L}_i$, $\hat{R}_i$

8.2. Choice of velocity α_{R_i}

If $\mathcal{S}_i\left(t_{k+1}\right) \notin \bar{\mathcal{S}}_i\left(\eta_i, t_k\right)$ and the reduction of L_i is not enough/possible, the velocity α_{R_i} is reduced to limit the motion of R_i, as described in Algorithm 4. This one is reduced several time but such as never reach $\alpha_{R_i} = 0$, where the situation would be blocked.

Algorithm 4 Choice of $\alpha_{R_i}\left(t_{k+1}\right)$

Require: $\vec{v}_{R_i}$, L_i, Need_Reduction_L
$\alpha_i^* = 1$, $\tilde{L}_i = L_i$ % by default
test = False, $n = 0$
while (test = False)&$(n < 7)$ **do**
  Calculation of $\hat{R}_i\left(t_{k+1}, \alpha_i^*, \vec{v}_{R_i}\right)$ using (17) % estimation next position of R_i
  Extend L_i if need/possible using Algorithm 3 $\rightarrow \tilde{L}_i$ and $\hat{R}_i$
  Calculation of $\mathcal{S}_i\left(t_{k+1}\right)$ using $\hat{R}_i$ and $\tilde{L}_i$
  if $\mathcal{S}_i\left(t_{k+1}\right) \notin \bar{\mathcal{S}}_i\left(\eta_i, t_k\right)$ **then**
    % reduction length L_i if possible
    if (Need_Reduction_L = False)&$(\mathcal{E}_i^L\left(t_{k+1}\right) \cap \bar{\mathcal{E}}_i^L\left(\eta_i, t_k\right) \neq \emptyset)$ **then**
      if $\left(L_i\left(t_k\right) - \delta L_{\max}\right) < \left\|O_iR_i\right\|\left(t_k\right) + V_{R_i\max}\Delta T$ **then**
        $\tilde{L}_i = L_i - \delta L_{\max}$
      end if
      Need_Reduction_L = $False$
    else
      % Reduction velocity α_i^*
      $n = n + 1$
      $\alpha_i^* = 0.6^n$ % Reduction of the velocity
    end if
  else
    test = True % end of the loop
  end if
end while
$L_i\left(t_{k+1}\right) = \tilde{L}_i$ % Update the length L_i
$\alpha_{R_i}\left(t_{k+1}\right) = \alpha_i^*$
return $\alpha_{R_i}\left(t_{k+1}\right)$ and $L_i\left(t_{k+1}\right)$

9. ROVs personality

9.1. The main idea

As stated by [9], introducing personality in a robot fleet can help to resolve conflicts because it introduces different behaviors in the group. When several robots try to avoid each other, having the exact same behavior and rules can lead to an impasse, as illustrated in Figure 11. In opposite, different behaviors can unlock situation by for example by giving the priority to another robot in all circumstances, even if in some situation it would be more efficient if all robot would be equal.

9.2. ROV's personality traits

An ROV/obstacle i is defined by three kind of personality traits $\mathrm{HAL}(i) = \left\{\mathrm{H}^i, \mathrm{A}^i, \mathrm{L}^i\right\}$ with $\mathrm{H}^i \geq 0$ the Hazardousness, $\mathrm{A}^i \geq 0$ the Aggressiveness and $\mathrm{L}^i \geq 0$ the Laziness. By default, an ROV i has a personality equal to $\mathrm{HAL}(i) = \{0, 0, 0\}$. Personality traits are defined as follow:

- **Hazardousness**: the more dangerous the ROV/obstacle i, the more ROVs try to keep their distance from it → when an other ROV j tests the collision with the ROV/object i, an additional layer $\bar{\mathcal{S}}_i\left(\eta_i + \mathrm{H}^i\right)$ is considered.
- **Aggressiveness**: if an ROV i is more aggressive that an ROV/obstacle j AND at least as hazardous, it will go straight to its target without try to bypass it → no bypass strategy if the ROV i is more aggressive than an ROV/obstacle j.
- **Laziness**: if an ROV i is lazier that an other ROV/obstacle j AND at least as aggressive, it will slow down during the collision avoidance to let the other makes the most part of the avoidance → reduction of the initial velocity α_i^* depending of the collision avoidance.

Different personalities can be arbitrarily assigned to help resolve potential conflicts. However, one can observe that

- A fixed ROV/obstacle j (Definition 4) have a personality of $\mathrm{HAL}(j) = \left\{\mathrm{H}^j, \infty, \infty\right\}$ with $\mathrm{H}^j \geq 0$ because it will never move, so the ROVs must bypass and avoid it. Same for obstacles which do not respect anti-collision strategies developed in this paper.
- A large hazardousness H can be given to
  - Items with a high velocity, *i.e.* larger risk of collision;

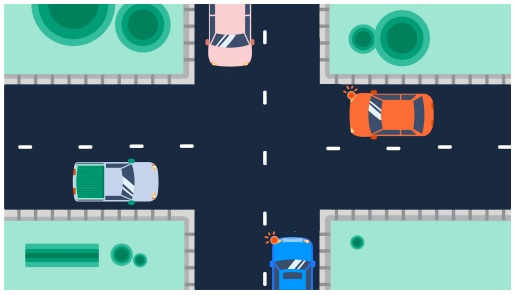

Figure 11: In this configuration, if all the cars want to go straight ahead but respect the rule "right of way" rule, the situation will remain eternally blocked. The same applies if all cars decide to ignore the rule and pass at the same time (crash). But if just one "aggressive" car forces its way through while the others stay "passive", the situation will be unblocked. Having different behavior can help to solve conflict.

  - Items whose collision must be avoided at all costs because they are truly hazardous like sharpest rock, an underwater mine, etc... or conversely a fragile item which must not be damaged;
  - A priority ROV whose we don't want to interfere the trajectory. Ideed, if $\mathrm{H}^i > \mathrm{H}^j$, ROV j will start to avoid ROV i before this one starts to react. A high aggressiveness can also be recommended in this case.

- Laziness can be used for ROV/vehicle which have difficulty maneuvering.

Remark 5. *Aggressiveness was created to avoid that several ROVs try indefinitely to bypass each other (frequent when three or more ROVs are involved). The Laziness was created to avoid large displacement which could lead to more collisions when several closed ROVs try to avoid each others. The Hazardousness was created to delay the detection of collision between several ROVs: the ROV with the smallest hazardousness will start to avoid the others before the other.*

Note that an aggressive ROV i compensates its absence of bypass strategy with a less aggressive ROV j by "pushing" the ROV j when it comes in contact: the ROV j will move from the ROV i using the repelling collision-avoidance strategy, bypassing ROV i if need. That's also why Hazardousness have the priority on Aggressiveness: an ROV i with a lower Hazardousness, and so layer, will react before ROV j and so cannot push the ROV j from its trajectory.

9.3. Personality rules

For two ROVs/obstacles (i, j), two tests of aggressiveness and laziness $\mathcal{T}_{\mathrm{Aggro}}(i,j)$ and $\mathcal{T}_{\mathrm{Lazy}}(i,j)$ are defined:

$$\mathcal{T}_{\mathrm{Aggro}}(i,j) = \text{True if } \left(\mathrm{A}^i > \mathrm{A}^j\right) \,\&\, \left(\mathrm{H}^i \geq \mathrm{H}^j\right) \tag{39}$$

$$\mathcal{T}_{\mathrm{Lazy}}(i,j) = \text{True if } \left(\mathrm{L}^i > \mathrm{L}^j\right) \,\&\, \left(\mathrm{A}^i \geq \mathrm{A}^j\right) \tag{40}$$

Based on these tests, the influences of the personality can be considered by adding the following rules:

- **Hazardousness**: the collision between an ROV i and an obstacle $\mathcal{A}^i_j$ is tested using $\bar{\mathcal{S}}_i(\eta_i) \cap \bar{\mathcal{A}}^i_j(\eta_j + \mathrm{H}^j)$;
- **Aggressiveness**: the condition $\mathcal{T}_{\mathrm{Aggro}}(i,j) = \text{True}$ is added to the "if" condition in line 5 in Algorithm 6;
- **Laziness**: for a chosen reduced velocity $0 < \alpha_{\mathrm{lazy}} < 1$, the Algorithm 5 is used to choose α_i^* at line 1 in Algorithm 4.

Note also that

- The initial and final positions of the ROVs must consider the layer of the Hazardousness H such that there is not collisions between ROVs (see Section 7.1 with the layer η).
- When an ROV i has reached its final position, it is recommend to change its layer η_i and hazardousness H^i to take it as small as possible to give space to others ROVs ($\eta = \mathrm{H}^i = 0$ if possible).
- The reduced velocity α_{lazy} must be strictly positive so that the ROV retains a minimum of movement between two iterations, otherwise the configuration may get stuck.

Remark 6. *(1) Aggressiveness is a way out of certain blocking situations, but there's no guarantee that it will lead to faster convergence.*

(2) If one takes $HAL(i) = \{0,0,0\}$ *for all ROVs, i.e. aggressiveness and laziness of all ROVs are equal, rules described in this section can be ignored.*

Algorithm 5 Velocity with laziness

Require: $\mathcal{L}^i_Q$
1: $L_{\alpha_i^*} = []$
2: **if** $\mathcal{L}^i_Q = \emptyset$ **then**
3: $\quad \alpha_i^* = 1$ % if no collision, maximum velocity
4: **else**
5: $\quad$ **for** j in $1 : N_{\mathrm{obs}}$ **do**
6: $\quad\quad$ **if** $Q_{ij} > 0$ **then**
7: $\quad\quad\quad$ **if** $\mathcal{T}_{\mathrm{Lazy}}(i,j) = \text{True}$ **then**
8: $\quad\quad\quad\quad$ % If ROV lazier, we take a slower velocity
9: $\quad\quad\quad\quad L_{\alpha_i^*} = [L_{\alpha_i^*}; \alpha_{\mathrm{lazy}}]$
10: $\quad\quad\quad$ **else**
11: $\quad\quad\quad\quad L_{\alpha_i^*} = [L_{\alpha_i^*}; 1]$
12: $\quad\quad\quad$ **end if**
13: $\quad\quad$ **end if**
14: $\quad$ **end for**
15: $\quad$ % We take the average velocity
16: $\quad \alpha_i^* = \mathrm{mean}\left(L_{\alpha_i^*}\right)$
17: **end if**
18: **return** α_i^*

10. Simulations

To illustrate the proposed strategy, several simulations were performed using one to three ROVs and several obstacles. First simulations were made without ROV personality (HAL $= \{0, 0, 0\}$ for all ROVs) to show the performance of the model, then the personalities were added to show the interest of them. The simulations have been made with Matlab2022b. The ROVs are modeled using the discret model (16) with the samping time $\Delta T = 1$ and maximal velocity $V_{R_i \max} = 0.25$: we can so consider each iteration of the system with the variable $k \in \mathbb{N}$.

Consider the following TMS parameters with the maximum roll-out/roll-in $\delta L_{\max} = 0.3$ of the TMS, the maximum chosen roll-out $\Delta L = 0.25$, and $\delta_L = 0.5$ such that $\forall t > 0$, $L_i(t) < \left\| O_i R_i^* \right\| + \delta_L$. Due to the last condition, we don't need to put a limit of tether length: $L_{i,\max} = \infty$.

A target R_i^* is considered as reached if one has $\left\| R_i - R_i^* \right\| < 0.3$, so a little larger than the maximum distance perform during an iteration: $V_{R_i \max} \Delta T = 0.25$.

By default, the layer is taken equal to $\eta_i = 0.3$ for the ROV $i \in \mathcal{N}$ and $\eta_i = 0$ for the fixed obstacles. Once an ROV i has reached its target, it is considered as a fixed obstacles ($A^i = \infty$ and $\alpha_i = 0$, *i.e.* cannot move), its layer becomes equal to $\eta_i = 0$ until a new target is assigned to it, but it can still modify its tether's length L_i if required. For all system $\mathcal{S}_i$, we consider the ellipsoid $\mathcal{E}_i^O$ and $\mathcal{E}_i^R$ containing O_i and R_i are sphere of radius $r = 0.1$. The layers of $\mathcal{E}_i^O$, $\mathcal{E}_i^L$ and $\mathcal{E}_i^R$ are equal to η_i. No collision has been detected in simulations performed.

10.1. One ROV and fixed obstacles

In this section, one ROV tries to reach its target R^* using collision avoidance strategies described in the paper. Seven examples of scenario are presented, illustrated in Figure 12. A video of these simulations is available at https://youtu.be/l8kwkpFDTKY with additional examples.

Example 1: Park between boats type "full-obstacle" In Figure 12a, the ROV 1 (in blue) tries to reach its target between two full obstacles on the surface, modeling two boats. The repelling strategy allows to avoid collision with the first boat, and the reduction of tether length allows to not come in contact with both boat when the ROV is between them.

Example 2 and 3: Fixed "tether obstacle" In Figures 12b and 12c, the ROV 1 (blue) uses the bypass strategy to avoid an other fixed ROV 2 (magenta) to reach its target. Intersection between $\mathcal{E}_1^L$ and $\mathcal{E}_2^L$ are allowed, but since the main axis of $\mathcal{E}_2^L$ is on the way of the ROV, it must bypass it to reach its target. In Figure 12c, repelling strategy used in parallel of bypass strategy allows to avoid collision with the seafloor (blue plane).

Example 4: square full-obstacle In Figure 12d, the only way to reach the ROV's target requires to pass inside a square obstacle (modeled by four ellipsoids): the bypass strategy has been automatically used to bypass one side of the square, *i.e.* center the ROV with the target, then the cable length is managed to pass inside without $\mathcal{E}^L$ touch the obstacles.

Example 5, 6 and 7: Bypass two vertical "tether obstacles" In Figure 12a, two fixed tethers block the path and cannot change their length. The tether of ROV 1 can touch them but the ROV itself cannot pass through. The bypass strategy cannot be activated because the main axis of both ellipsoids are not on the way. However, using the repelling strategy, the ROV runs along the surface of the two ellipsoids to pass over them.

In the other examples exposed in Figure 13c (video at https://youtu.be/ztTy3B6FP5o), the same configuration is proposed but where the two ROVs obstacles can change their tether's length. The solution found is different: the two ROVs reduce their tethers and allow to let the first ROV passes between them.

However, some limits of the method can be shown with a similar configuration: in example illustrated in Figure 13d, an additional horizontal plane has been added below the two obstacles (which cannot change their tether's length here) and target has been slightly down. The ROV tries to reach it by the shortest path leading by the bottom to the two obstacles, but it is blocked by the seafloor and cannot find an escape. This problem is unfortunately common to all APF as the repulsive forces used in the repelling strategy. A method of type "path-planing" would be required to solve this problem.

10.2. Two ROVs simulations

Four scenarios with two moving ROVs avoiding themselves are illustrated in Figure 17. The video of these simulations is available at https://youtu.be/MVhnOfxujIY . In these examples, the ROVs try to reach two successive target R^*: when all ROVs have reached their first target, the second target is activated.

The Figure 14 shows a scenario where the cable between an ROV $i \in \{1, 2\}$ and the boat is modeled in two parts: a first part considering the cable between the ROV R_i and the anchor O_i as a system $\mathcal{S}_i$, and a second part considering the cable between the anchor O_i and a boat on the surface as a full obstacle i' noted $\mathcal{S}_{i'}$ (same color on the figure that $\mathcal{S}_i$). One has $\mathcal{E}_i^O = \mathcal{E}_{i'}^O$, collisions between $\mathcal{E}_i^L$, $\mathcal{E}_{i'}^L$, $\mathcal{E}_i^O$ and $\mathcal{E}_{i'}^O$ are not considered, but collisions between $\mathcal{E}_i^R$ and $\mathcal{S}_{i'}$ are.

Case 1: without personality In Figure 14a, personalities are not considered. The two ROVs try to reach their first target placed behind the other ROV: they need first to avoid each other, inducing one of the two ROVs j will be trapped between $\mathcal{S}_i$ and $\mathcal{S}_{i'}$. Then, to reach the second target, the paths of the two ROVs must cross again. In this case, the ROV 1 must bypass the ROV 2 which takes the shortest path and so is on ROV 1's path. Then, when the path is clear, ROV 1 can go straight to its target.

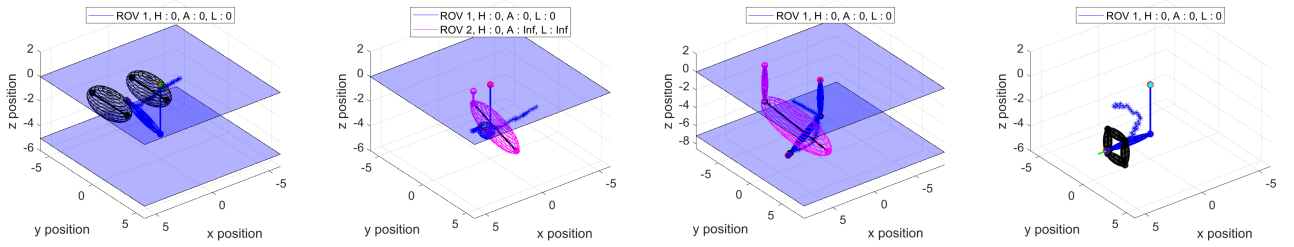

(a) ROV 1 avoiding two boats (black obstacles) on the surface to reach the target between them.

(b) ROV 1 avoiding an other fixed ROV to reach its target.

(c) ROV 1 avoiding an other fixed ROV to reach its target.

(d) ROV avoiding a square obstacle to reach its target.

Figure 12: Simulations with one moving ROV and several obstacles. Blue ellipsoid: tether 1. Magenta ellipsoid: tether 2 obstacle. Black ellipsoids: full-obstacles. Blue plane: sea surface.

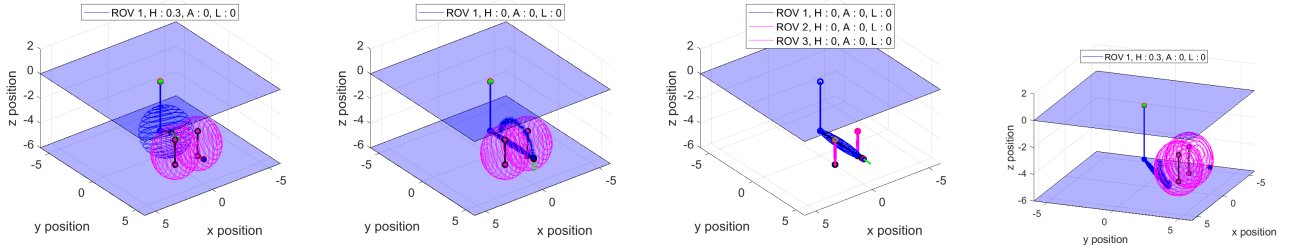

(a) Initial position

(b) ROV 1 bypass two fixed tether obstacles which cannot change their lengths

(c) Tethers 2 and 3 s are allowed to reduce their tethers: the target is reached faster because they let through tether 1

(d) Here, the target is a little lower: the shortest path leads to the bottom of the two tether obstacles. ROV 1 is blocked by the seafloor and cannot find an escape.

Figure 13: ROV 1 bypassing two ROVs 2 and 3. Blue ellipsoid: tether 1. Magenta ellipsoids: tethers 2 and 3. Blue planes: sea surface and seafloor.

Case 2: Laziness When the personalities are added to ROVs, the paths follow by ROVs differ. In Figure 14b, Laziness has been added to ROV 1 ($L^1 = 4$ and $L^2 = 3$). The distance between ROVs and their targets (Figure 14f) shows that for $k \in [40, 60]$ the distance between ROV 1 and its target reduces faster than in case 1: the slowdown gives ROV 2 time to pass, so that it deviates less from the most direct trajectory. Note the contribution of this personality trait is minimal: it is more interesting when more ROVs are involve.

Case 3: Hazardousness In Figure 14c, a higher Hazardousness has been given to ROV 1($H^1 = 0.45$ and $H^2 = 0.3$). The distance between ROVs and their targets (Figure 14g) shows that for $k \in [0, 40]$, *i.e.* when ROVs try to reach their first target, ROV 1 go straight to its target while ROV 2 must move away for a time ($k \in [15, 30]$) to avoid ROV 1: the addition of Hazardousness has changed the priority because ROV 2 tries to avoid ROV 1 before this one did. Note that the path to the second target remains globally unchanged because ROV 1 still try to bypass ROV 2 on this path.

Case 4: Aggressiveness In Figure 14d, a higher Aggressiveness has been given to ROV 1 ($A^1 = 4$ and $A^2 = 3$). The the distance between ROVs and their targets (Figure 14h) shows that the path to the first target remains unchanged compare to case 1, but ROV 1 goes straight to its second target ($k \in [45, 90]$) while ROV 2 must avoid it ($k \in [55, 65]$): due the Aggressiveness, ROV 1 does not use the bypass strategy and pushes ROV 2 back from its shortest path.

A case not shown here but tested is the fusion of all personality traits: $\mathrm{HAL}(1) = \{0.45, 4, 4\}$ and $\mathrm{HAL}(2) = \{0.3, 3, 3\}$. In this case, the ROV 1 goes straight to these two targets with very small deviations while the ROV 2 must avoid it by reaching its target by a longest path.

10.3. Three ROVs simulations

Three ROVs with "tether obstacle" collisions In Figure 17a, three ROVs tries to reach simultaneously their targets to form the bisectors of a triangle, then switch their positions to reach the target position of the ROV on its right. It leads to several path intersections, each one trying to avoid/bypassing each other. The collision between ROVs are considered as "tether obstacle", so intersection between

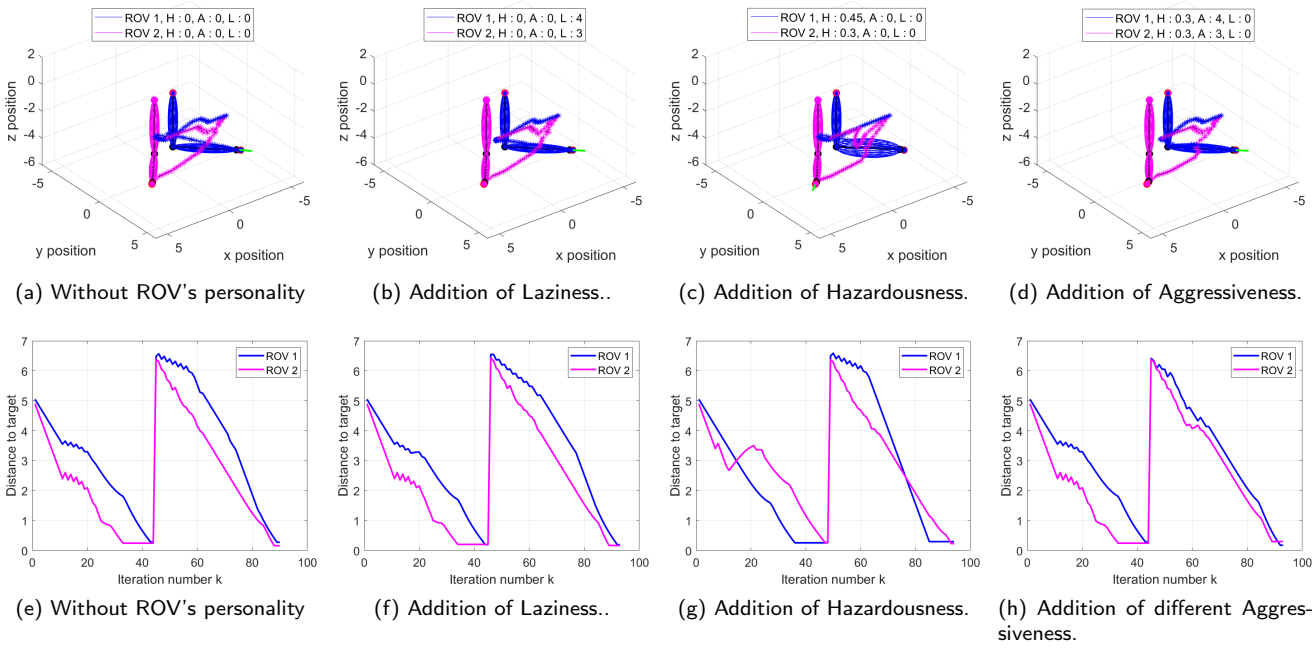

(a) Without ROV's personality (b) Addition of Laziness.. (c) Addition of Hazardousness. (d) Addition of Aggressiveness.

(e) Without ROV's personality (f) Addition of Laziness.. (g) Addition of Hazardousness. (h) Addition of different Aggressiveness.

Figure 14: Simulations with two ROVs. Both ROVs must reach a first target, then a second one. The targets always induce to cross the trajectory of the other ROV. Magenta ellipsoid: tether 1. Blue ellipsoid: tether 2.

ellipsoids $\mathcal{E}^L$ are allowed. An equilibrium can be found after some time, but this one is difficult to find.

The introduction of the personalities, illustrated in Figure 17f, leads to a faster solution: by taking $\mathrm{HAL}(1) = \{0.6, 3, 3\}$, $\mathrm{HAL}(2) = \{0.45, 2, 2\}$ and $\mathrm{HAL}(3) = \{0.3, 1, 1\}$, ROV 1 finds this way first, then ROV 2 and finally ROV 3. Each time an ROV reaches its target and so stops to move, it is easier for other ROVs to find their way.

The video of these simulations is available at https://youtu.be/No91xVVsZv4 .

Three ROVs with "full obstacle" collisions In this second examples illustrate in Figure 17k and Figure 17p, the collisions between ROVs are now considered as "full obstacle", so intersections between systems $\mathcal{S}$ are not allowed. This situation is much more complex because tethers have to keep greater distances between them. The depth of targets have been adapted such that there is not collision between ROVs when they have reached their target. However, in the scenario without personality in Figure 17k, the ROVs cannot reach their targets because they block each other. However, by adding the personalities as in Figure 17k, a solution is found because some ROVs have priority over others.

Note an other modification has been made compare to previous examples: the velocity $V_{R_i \max}$ has been reduced such that $V_{R_i \max} = 0.125$ (and so $\Delta L = 0.125$) to take a smaller layer $\eta = 0.15$. Indeed, a too large layer is more a disadvantage than a help, because it induces a larger collision area to avoid, which can block the path to the target. Reducing speed reduces layer size, and so help to solve some configurations. A method to chose the most adapted velocity in function of the configuration (and not only during the avoidance like the Laziness), will be the subject of future studies.

The video of these simulations is available at https://youtu.be/AL9_agE7frQ .

11. Conclusion

This paper proposes a guarantee ellipsoid model of the ROV's tether and its obstacles to perform a collision avoidance method for a fleet of ROVs low in calculation. This model, which assimilate the ROV and its tether as a set of ellipsoids, guarantees that if an obstacle is not inside or partially inside the ellipsoid model, then the tether is guarantee to not collide with that obstacle. This model is pessimist but simple and can provide a guaranteed proof of non-collision without any knowledge of the tether shape or its dynamic, only its two attachments point and its length. A collision avoidance strategy has been developed specifically for ROVs and their tethers: it is based on potential field methods, tether's length management, and a bypass strategy. The bypass strategy allows to detect and get around an obstacle when this one is directly on the path between the system ROV+tether and its target position. Simulations show that these simple mechanisms can solve complex situations as long as it is not require to bend the cable on an obstacle (behavior forbidden in this study) to reach the target. When several ROVs are involved, personalities are added to ROV's to obtain different behaviors in the same configuration, and so limit the case of minimal local during collisions avoidance. Three kind of personality traits have been proposed: Hazardousness, Aggressiveness and Laziness. Simulations show Hazardousness and Aggressiveness allows to change

the priority between ROVs and solve configurations which could remain blocked, while the Laziness allows to smooth the collision avoidance but without offer an alternative solution.

Next studies will try to combine the proposed model with the path planing methods based on homotopy to solve more complex configurations. In case where a bend would be allowed with an obstacle, the model could also be divided into two ellipsoids to obtain a more flexible model.

References

[1] S. Alfano and M. L. Greer. Determining if two solid ellipsoids intersect. *Journal of guidance, control, and dynamics*, 26(1):106–110, 2003.

[2] R. Arnold, J. Jablonski, B. Abruzzo, and E. Mezzacappa. Heterogeneous uav multi-role swarming behaviors for search and rescue. In *In Proc IEEE CogSIMA*, pages 122–128, 2020.

[3] S. Bhattacharya, S. Kim, H. Heidarsson, G. S. Sukhatme, and V. Kumar. A topological approach to using cables to separate and manipulate sets of objects. *The International Journal of Robotics Research*, 34(6):799–815, 2015.

[4] O. Blintsov. Development of the mathematical modeling method for dynamics of the flexible tether as an element of the underwater complex. *Eastern-European Journal of Enterprise Technologies*, 1 (7):4–14, 2017.

[5] B. Buckham and M. Nahon. Dynamics simulation of low tension tethers. In *IEEE Conference Proceedings Oceans*, volume 2, pages 757–766, 1999.

[6] D. Bulić, D. Tolić, and I. Palunko. Beam-based tether dynamics and simulations using finite element model. *In Proc. IFAC-PapersOnLine*, 55(15):154–159, 2022.

[7] M. Cao, K. Cao, S. Yuan, T-M Nguyen, and L. Xie. Neptune: nonentangling trajectory planning for multiple tethered unmanned vehicles. *In Proc IEEE Transactions on Robotics*, 39(4):2786–2804, 2023.

[8] C. Cheng, Q. Sha, B. He, and G. Li. Path planning and obstacle avoidance for auv: A review. *Ocean Engineering*, 235:109355, 2021.

[9] Y. Ding, M. Zhu, Y. He, and J. Jiang. Using personality to avoid conflict in the multi-robot system. In *International Conference on Control, Automation, Robotics and Vision*, pages 1–6, 2006.

[10] J. Drupt, C. Dune, A. I. Comport, and V. Hugel. Validity of the catenary model for moving submarine cables with negative buoyancy. In *3rd workshop on RObotic MAnipulation of Deformable Objects: challenges in perception, planning and control for Soft Interaction (ROMADO-SI)*, 2022.

[11] J. Drupt, C. Dune, A. I Comport, S. Seillier, and V. Hugel. Inertial-measurement-based catenary shape estimation of underwater cables for tethered robots. In *In proc. IEEE/RSJ International Conference on Intelligent Robots and Systems (IROS)*, pages 6867–6872, 2022.

[12] O. A. Eidsvik and I. Schjølberg. Time domain modeling of rov umbilical using beam equations. *IFAC*, 49(23):452–457, 2016.

[13] O. A. N. Eidsvik and I. Schjølberg. Finite element cable-model for remotely operated vehicles (rovs) by application of beam theory. *Ocean Engineering*, 163:322–336, 2018.

[14] M. Filliung, J. Drupt, C. Peraud, C. Dune, N. Boizot, A. Comport, C. Anthierens, and V. Hugel. An augmented catenary model for underwater tethered robots. In *In Proc. IEEE ICRA*, 2024.

[15] O. Ganoni, R. Mukundan, and R. Green. Visually realistic graphical simulation of underwater cable. *Computer Science Research Notes*, 2018.

[16] F. González, A. de la Prada, A. Luaces, and M. González. Real-time simulation of cable pay-out and reel-in with towed fishing gears. *Ocean Engineering*, 131:295–307, 2017.

[17] O. Hamed, M. Hamlich, and M. Ennaji. Hunting strategy for multi-robot based on wolf swarm algorithm and artificial potential field. *Indones. J. Electr. Eng. Comput. Sci*, 25(1):159, 2022.

[18] M. Ho, S. El-Borgi, D. Patil, and G. Song. Inspection and monitoring systems subsea pipelines: A review paper. *Structural Health Monitoring*, 19(2):606–645, 2020.

[19] Sung Min Hong, Kyoung Nam Ha, and Joon-Young Kim. Dynamics modeling and motion simulation of usv/uuv with linked underwater cable. *Journal of Marine Science and Engineering*, 8(5):318, 2020.

[20] S. Kim, S. Bhattacharya, and V. Kumar. Path planning for a tethered mobile robot. In *IEEE International Conference on Robotics and Automation (ICRA)*, pages 1132–1139, 2014.

[21] Y. Koren, J. Borenstein, et al. Potential field methods and their inherent limitations for mobile robot navigation. In *Icra*, volume 2, pages 1398–1404, 1991.

[22] R. Kot. Review of collision avoidance and path planning algorithms used in autonomous underwater vehicles. *Electronics*, 11(15):2301, 2022.

[23] Q. Li, L-J Wang, B. Chen, Z. Zhou, and Y-X Yin. An improved artificial potential field method with parameters optimization based on genetic algorithms. *Chinese Journal of Engineering*, 34(2):202–206, 2012.

[24] S. McCammon and G. A. Hollinger. Planning and executing optimal non-entangling paths for tethered underwater vehicles. In *In Proc IEEE ICRA*, pages 3040–3046, 2017.

[25] Ramon E Moore, R Baker Kearfott, and Michael J Cloud. *Introduction to interval analysis*. SIAM, 2009.

[26] T. Recchia, J. Chung, and K. Pochiraju. Improving learning in robot teams through personality assignment. *Biologically Inspired Cognitive Architectures*, 3:51–63, 2013.

[27] T. Recchia, J. Chung, and K. Pochiraju. Performance of heterogeneous robot teams with personality adjusted learning. *Biologically Inspired Cognitive Architectures*, 7:87–97, 2014.

[28] M. Such, J. R. Jimenez-Octavio, A. Carnicero, and O. Lopez-Garcia. An approach based on the catenary equation to deal with static analysis of three dimensional cable structures. *Engineering structures*, 31(9):2162–2170, 2009.

[29] G. Tan, J. Zhuang, J. Zou, L. Wan, and Z. Sun. Artificial potential field-based swarm finding of the unmanned surface vehicles in the dynamic ocean environment. *International Journal of Advanced Robotic Systems*, 17(3):1729881420925309, 2020.

[30] K. Teo, K. W. Ong, and H. C. Lai. Obstacle detection, avoidance and anti collision for meredith auv. In *OCEANS*, pages 1–10, 2009.

[31] C. Viel. Self-management of rov umbilical using sliding buoys and stop. *IEEE Robotics and Automation Letters*, 7(3):8061–8068, 2022.

[32] C. Viel. Self-management of the umbilical of a rov for underwater exploration. *Ocean Engineering*, 248:110695, 2022.

[33] C. Viel. Self-management of rov umbilical using sliding element: A general 3d-model. *Applied Ocean Research*, 151:104164, 2024.

[34] Christophe Viel. Self-Management of ROV Umbilical using sliding element: a general 3D-model - Full version. working paper or preprint. https://hal.science/hal-04157011, July 2023.

[35] Z. Yu, J. Yuan, Y. Li, C. Yuan, and S. Deng. A path planning algorithm for mobile robot based on water flow potential field method and beetle antennae search algorithm. *Computers and Electrical Engineering*, 109:108730, 2023.

[36] X. Zhang and Q-C Pham. Planning coordinated motions for tethered planar mobile robots. *Robotics and Autonomous Systems*, 118:189–203, 2019.

A. Mathematical tools

A.1. Calculation closest points between segments

In this section, a method to evaluate the two closest points between two segments is proposed, summarized in Theorem 10. To increase the clarity of the results, the results

have been separated into several small theorems and definitions described below. Theorem 8 provides the closest points between two lines. Definition 9 provides a test to check if a point on a line is inside a segment. Theorem 9 provides the closest point on a line or segment to another single point. Proves of these theorems can be found in Appendix B.4.1.

Theorem 8. *For two lines (O_1R_1) and (O_2R_2), let $\vec{V}_k = R_k - O_k$ be the main vectors with $k \in [1,2]$. Let define $V_3 = V_2 \wedge V_1$ the mutual orthogonal vector to (O_1R_1) and (O_2R_2). The closest points between the two lines $Q_1 \in (O_1R_1)$ and $Q_2 \in (O_2R_2)$ can be expressed as*

$$Q_1 = O_1 + t_1\vec{V}_1 \tag{41}$$

$$Q_2 = O_2 + t_2\vec{V}_2 \tag{42}$$

where $\{t_1, t_2\} \in \mathbb{R}^2$ are solutions of the following system

$$\begin{cases} t_3 v_{x3} - t_2 v_{x2} + t_1 v_{x1} &= x_{O,2} - x_{O,1} \\ t_3 v_{y3} - t_2 v_{y2} + t_1 v_{y1} &= y_{O,2} - y_{O,1} \\ t_3 v_{z3} - t_2 v_{z2} + t_1 v_{z1} &= z_{O,2} - z_{O,1} \end{cases} \tag{43}$$

with $\forall i \in [1,2,3]$ $\vec{V}_i = \begin{bmatrix} v_{x,i} & v_{y,i} & v_{z,i} \end{bmatrix}^T$ and $O_i = \begin{bmatrix} x_{O,i} & y_{O,i} & z_{O,i} \end{bmatrix}^T$, and where t_3 the third unknown variable of (43).

Proof of Theorem 8 is provided in Appendix B.4.1.

The following Definition 9 provides a test to check if a point P_1 is on a segment $[O_1R_1]$.

Definition 9. *Suppose $P_1 \in (O_1R_1)$ a point on the line (O_1R_1). One can deduce that*

(1) If $(\|P_1O_1\| \leq \|O_1R_1\|)$ & $(\|P_1R_1\| \leq \|O_1R_1\|)$, P_1 is a point of the segment $[O_1R_1]$, i.e. $P_1 \in [O_1R_1]$;

(2) If $(\|P_1O_1\| > \|P_1R_1\|)$ & $(\|P_1O_1\| > \|O_1R_1\|)$, P_1 is not on the segment , i.e. $P_1 \notin [O_1R_1]$, and the closest extremity is R_1;

(3) If $(\|P_1O_1\| < \|P_1R_1\|)$ & $(\|P_1R_1\| > \|O_1R_1\|)$, P_1 is not on the segment , i.e. $P_1 \notin [O_1R_1]$, and the closest extremity is O_1.

The following Theorem 9 provides the closest point on a line or segment to another single point.

Theorem 9. *Consider a point P_2. Let define O_1 and R_1 defining a line (O_1R_1) or a segment $[O_1R_1]$ with $\vec{V}_1 = \vec{O_1R_1} = O_1 - R_1$ the main vector of the line/segment. One can define*

(1) S_1 the closest point of P_2 on the line (O_1R_1) where $S_1 = O_1 + \left(\frac{\vec{V}_1.P_2 - \vec{V}_1.O_1}{\|\vec{V}_1\|^2}\right)\vec{V}_1$;

(2) $\bar{S}_1$ the closest point of P_2 on the segment $[O_1R_1]$ where

$$\bar{S}_1 = \begin{cases} R_1 & \text{if } (\|S_1O_1\| > \|O_1R_1\|) \,\&\, (\|S_1O_1\| > \|S_1R_1\|) \\ O_1 & \text{if } (\|S_1R_1\| > \|O_1R_1\|) \,\&\, (\|S_1O_1\| < \|S_1R_1\|) \\ S_1 & \text{else.} \end{cases} \tag{44}$$

Proof of Theorem 9 is provided in Appendix B.4.2.

Combining previous definitions and theorems, following Theorem 10 provides a method to evaluate the two closest points between two segments.

Theorem 10. *Let define the two segments $[O_1R_1]$ and $[O_2R_2]$ with $O_1 \neq R_1$ and $O_2 \neq R_2$. Let define $Q_1$and Q_2 the closest points between the two lines (O_1R_1) and (O_2R_2) as defined in Theorem 8. The two closest points $\bar{S}_1 \in [O_1R_1]$ and $\bar{S}_2 \in [O_2R_2]$ between $[O_1R_1]$ and $[O_2R_2]$ can be expressed as following:*

(1) If $Q_1 \in [O_1R_1]$ and $Q_2 \in [O_2R_2]$, then one has $\bar{S}_1 = Q_1$ and $\bar{S}_2 = Q_2$.

(2) If $Q_1 \notin [O_1R_1]$ or $Q_2 \notin [O_2R_2]$, at least one of $\bar{S}_1$ and $\bar{S}_2$ is an extremity of segments $[O_1R_1]$ and $[O_2R_2]$. The couple of closest points can so be expressed as

$$(\bar{S}_1, \bar{S}_2) = \begin{cases} \left(\bar{S}_1^{(1)}, \bar{S}_2^{(1)}\right) & \text{if } \left\|\bar{S}_1^{(1)}\bar{S}_2^{(1)}\right\| < \left\|\bar{S}_1^{(2)}\bar{S}_2^{(2)}\right\| \\ \left(\bar{S}_1^{(2)}, \bar{S}_2^{(2)}\right) & \text{else.} \end{cases} \tag{45}$$

where

$$\bar{S}_1^{(1)} = \begin{cases} R_1 & \text{if } (\|Q_1O_1\| > \|O_1R_1\|) \,\&\, (\|Q_1O_1\| > \|Q_1R_1\|) \\ O_1 & \text{if } (\|Q_1R_1\| > \|O_1R_1\|) \,\&\, (\|Q_1O_1\| < \|Q_1R_1\|) \\ Q_1 & \text{else} \end{cases} \tag{46}$$

$$\bar{S}_2^{(2)} = \begin{cases} R_2 & \text{if } (\|Q_2O_2\| > \|O_2R_2\|) \,\&\, (\|Q_2O_2\| > \|Q_2R_2\|) \\ O_2 & \text{if } (\|Q_2R_2\| > \|O_2R_2\|) \,\&\, (\|Q_2O_2\| < \|Q_2R_2\|) \\ Q_2 & \text{else} \end{cases} \tag{47}$$

and $\bar{S}_2^{(1)}/\bar{S}_1^{(2)}$ are evaluated using Theorem 9 with $\bar{S}_1^{(1)}/\bar{S}_2^{(2)}$.

Proof of Theorem 10 is provided in Appendix B.4.3.

A.2. Theorem Intersection between plane and ellipsoid

The intersection between a plane $\mathcal{P}$ and an ellipsoid $\mathcal{E}_i$, if it exists, is an ellipse in the plane $\mathcal{P}$: the Theorem 11 provides a test which check if this ellipse exists, and so deduce if $\mathcal{E}_i \cap \mathcal{P} \neq \emptyset$.

Theorem 11. *Consider a plane $\mathcal{P}(P, \vec{n})$ as expressed in Definition 5 and an ellipsoid of revolution $\mathcal{E}_i$ as defined in*

Definition 2. The intersection between $\mathcal{P}$ and $\mathcal{E}_i$ exist, i.e. $\mathcal{E}_i \cap \mathcal{P} \neq \emptyset$, if the following condition (48) is satisfied:

$$\left(T_1 \geq 0\right) \& \left(T_2 \geq 0\right) \tag{48}$$

where

$$T_1 = A_0 C_0 - B_0^2 \tag{49}$$

$$T_2 = \left(B_0 D_0 - A_0 E_0\right)^2 - \left(D_0^2 - A_0 F_0\right)\left(B_0^2 - A_0 C_0\right) \tag{50}$$

with

$$A_0 = \frac{\bar{\alpha}^2}{\bar{\gamma}^2} + \frac{c^2}{a^2} \quad B_0 = \frac{\bar{\alpha}\bar{\beta}}{\bar{\gamma}^2}$$
$$C_0 = \frac{\bar{\beta}^2}{\bar{\gamma}^2} + \frac{c^2}{b^2} \quad D_0 = \frac{\bar{\alpha}\bar{\delta}}{\bar{\gamma}^2}$$
$$E_0 = \frac{\bar{\beta}\bar{\delta}}{\bar{\gamma}^2} \qquad F_0 = \frac{\bar{\delta}^2}{\bar{\gamma}^2} - c^2$$

and $\bar{\delta} = -\left(\bar{\alpha}\bar{x}_P + \bar{\beta}\bar{y}_P + \bar{\gamma}\bar{z}_P\right)$ evaluated using $\vec{n} = \begin{bmatrix} \bar{\alpha} & \bar{\beta} & \bar{\gamma} \end{bmatrix}^T$ and $\bar{P} = \left[\bar{x}_P, \bar{y}_P, \bar{z}_P\right]^T$ expressed as

$$\bar{P}_{\mathcal{R}_i} = \boldsymbol{M_c}^i \left(P - C_{i|\mathcal{R}}\right) \tag{51}$$

$$\vec{\bar{n}}_{\mathcal{R}_i} = \boldsymbol{M_c}^i \vec{n}_{\mathcal{R}} \tag{52}$$

where $\boldsymbol{M_c}^i$ associated to $\mathcal{E}_i$ as be defined in Definition 2.

Else, if (48) not satisfy, one has $\mathcal{E}_i \cap \mathcal{P} = \emptyset$.

Proof of Theorem 11 is provided in Appendix B.5.

A.3. Theorem obstacle on the path

The following Theorem 12 provides a method to check the conditions of Definition 8, *i.e.* if there is an obstacle on the path.

Theorem 12. *For a system $\mathcal{S}_i$ and following Definition 8, an ellipsoid $\mathcal{E}_{obs}$ is on the path between $\boldsymbol{R}_i$ and its target $\boldsymbol{R}_i^*$ if the three following conditions are satisfied:*

(1) $\vec{V}_{obs}.\vec{n}_k \neq 0$ where $\vec{V}_{obs} = \vec{F_{1,obs}F_{2,obs}}$ and $\vec{n}_k = \vec{O_iR_i} \wedge \vec{O_iR_i^*}$;

(2) $P_a \in \left[F_{1,obs}F_{2,obs}\right]$ where $P_a = \begin{bmatrix} x_a & y_a & z_a \end{bmatrix}^T$ is the solution of the system

$$\begin{cases} t\upsilon_x + x_{F_{1,obs}} & = x_a \\ t\upsilon_y + y_{F_{1,obs}} & = y_a \\ t\upsilon_z + z_{F_{1,obs}} & = z_a \\ \alpha_k x_a + \beta_k y_a + \gamma_k z_a & = 0 \end{cases} \tag{53}$$

where x_a, y_a, z_a and t are the unknown variables with $F_{1,obs} = \begin{bmatrix} x_{F_{1,obs}} & y_{F_{1,obs}} & z_{F_{1,obs}} \end{bmatrix}^T$,

$\vec{F_{1,obs}F_{2,obs}} = \begin{bmatrix} \upsilon_x & \upsilon_y & \upsilon_z \end{bmatrix}$, $\vec{n}_k = \begin{bmatrix} \alpha_k & \beta_k & \gamma_k \end{bmatrix}^T$ and $\delta_k = -\left(\alpha_k x_{O,i} + \beta_k y_{O,i} + \gamma_k z_{O,i}\right)$;

(3) $T_3 = 0$ with

$$T_3 = \mathcal{A}_{O_iR_iR_i^*} - \left(\mathcal{A}_{O_iR_iP_a} + \mathcal{A}_{O_iP_aR_i^*} + \mathcal{A}_{P_aR_iR_i^*}\right) \tag{54}$$

where $\mathcal{A}_{ABC} = \frac{\left\|\vec{AB} \wedge \vec{AC}\right\|}{2}$ is the area of a triangle ABC.

Proof of Theorem 12 is provided in Appendix B.6. The test $P_a \in \left[F_{1,\text{obs}}F_{2,\text{obs}}\right]$ can be performed using Definition 9 in Appendix A.1.

A.4. Theorem calculation of the tangent circle $C^{i,j}_{\text{tangent}}$

For each obstacle $\mathcal{E}^{i,j}_{\text{obs}} \in \mathcal{L}^i_{\mathcal{O}\text{bypass}}(t)$, we can define a circle $C^{i,j}_{\text{tangent}}\left(\mathcal{E}^{i,j}_{\text{obs}}, O_i, r^{i,j}_{\text{tangent}}\right)$ tangent to $\mathcal{E}^{i,j}_{\text{obs}}$, centered in O_i and with a radius $r^{i,j}_{\text{tangent}}$, as illustrated in green in Figure 9 and which can be evaluated using Theorem 13.

Theorem 13. *For a system $\mathcal{S}_i$ and an ellipsoid obstacle $\mathcal{E}_j$, the circle $C^{i,j}_{tangent}\left(\mathcal{E}_j, O_i, r^{i,j}_{tangent}\right)$ center in O_i is tangent to $\mathcal{E}_j$ with the radius $r^{i,j}_{tangent}$ expressed as*

$$r^{i,j}_{tangent} = \min_{X_{(k)} \in S_X}\left(\sqrt{X^T_{(x)}X_c}\right) \tag{55}$$

where $X_c = \boldsymbol{M_c}^j\left(O_{i|\mathcal{R}} - C_{j|\mathcal{R}}\right)$ the coordinate of O_i in $\mathcal{R}_j$, $S_X = \left\{X_{(k)} \middle| k \in \left[1 \dots N_s\right], Im\left(X_{(k)}\right) = 0\right\}$ is the set of the N_s possible solution of the following system

$$\begin{cases} b_j^2\left(y_{(k)} - y_c\right)\left(z_{(k)} - z_c\right) & = c_j^2\left(z_{(k)} - z_c\right)\left(y_{(k)} - y_c\right) \\ c_j^2\left(z_{(k)} - z_c\right)\left(x_{(k)} - x_c\right) & = a_j^2\left(x_{(k)} - x_c\right)\left(z_{(k)} - z_c\right) \\ \frac{\left(x_{(k)} - x_c\right)^2}{a_j^2} + \frac{\left(y_{(k)} - y_c\right)^2}{b_j^2} & = 1 - \frac{\left(z_{(k)} - z_c\right)^2}{c_j^2} \end{cases} \tag{56}$$

with $X_c = \begin{bmatrix} x_c & y_c & z_c \end{bmatrix}^T$ and $X_{(k)} = \begin{bmatrix} x_{(k)} & y_{(k)} & z_{(k)} \end{bmatrix}^T$.

The proof of Theorem 13 is provided in Appendix B.8. Note that $\mathcal{E}_j$ must be replaced by $\bar{\mathcal{E}}_j$ in Theorem 13 to avoid the detection of collision.

A.5. Algorithm summarized target choice

The choice of $\hat{R}_i^*(t)$ and the bypass strategy is summarized in Algorithm 6 in Appendix .

B. Prove of theorems

B.1. Proof Definition 2

The coordinate of F_1^i and F_2^i are supposed known in $\mathcal{R}$. The ellipsoid of revolution $\mathcal{E}_i$ can be expressed in $\mathcal{R}_i$ as

$$\frac{x^2_{\mathcal{R}_i}}{a_i^2} + \frac{y^2_{\mathcal{R}_i}}{b_i^2} + \frac{z^2_{\mathcal{R}_i}}{c_i^2} = 1. \tag{57}$$

Algorithm 6 Choice of target $\hat{R}_i^*$: bypass strategy

Require: $\mathcal{L}^i_{\text{obs}}$
$\mathcal{L}^i_{\mathcal{O}\text{bypass}}(t) = \emptyset$
$\mathcal{L}^i_{r,\text{tangent}}(t) = \emptyset$
% Creation of the list of obstacles on the path
for j in $1 : N_{\text{obs}}$ **do**
  $\mathcal{E}^{i,j}_{\text{obs}} = \mathcal{L}^i_{\text{obs}}(j)$
  if $(\mathcal{E}^{i,j}_{\text{obs}} \notin \mathcal{L}_P) \& (d_j \cap O_i R_i R_i^* \neq \emptyset)$ **then**
    $\mathcal{L}^i_{\mathcal{O}\text{bypass}}(t) \leftarrow \mathcal{E}^{i,j}_{\text{obs}}$
    Evaluation of $r^{i,j}_{\text{tangent}}$ using (55)
    $\mathcal{L}^i_{r,\text{tangent}}(t) \leftarrow r^{i,j}_{\text{tangent}}$
  end if
end for
% Choice of the target
if $\mathcal{L}^i_{\mathcal{O}\text{bypass}}(t) = \emptyset$ **then**
  $\hat{R}_i^* = R_i^*$ % if no obstacle on the path
else
  Evaluation of r^i_{bypass} using (32)
  Evaluation of $\hat{R}_i^*(t)$ using (34)
end if
return $\hat{R}_i^*$

Evaluation of matrix $\boldsymbol{M_c}^i$ Let's define θ_i and ψ_i the orientation of vector $\vec{F_1F_2}$ in $\mathcal{R}$ such that

$$\theta_i = \text{atan2}\left(y_{F_2,i} - y_{F_1,i}, x_{F_2,i} - x_{F_1,i}\right) \tag{58}$$

$$\psi_i = \begin{cases} \text{asin}\left(\frac{z_{F_2,i} - z_{F_1,i}}{\|F_{1,i}F_{2,i}\|}\right) & \text{if } \|F_{1,i}F_{2,i}\| > 0 \\ 0 & \text{else} \end{cases} \tag{59}$$

and note that $\frac{F_{1,i}\vec{F}_{2,i}}{\left\|F_{1,i}\vec{F}_{2,i}\right\|} = \frac{\vec{a}_i}{\|a_i\|}$. Since $\mathcal{E}_i$ is an ellipsoid of revolution around $\vec{a}$, *i.e.* $b_i = c_i$, a third rotation is unnecessary.

Let's define the vector $X_{\mathcal{R}_i} = \begin{bmatrix} x_{\mathcal{R}_i} & y_{\mathcal{R}_i} & z_{\mathcal{R}_i} \end{bmatrix}$ and the rotation matrices $\boldsymbol{R}\left(\theta_i\right)_{y_i}$ and $\boldsymbol{R}\left(\psi_i\right)_{z_i}$ around axis $\vec{b}_i$ and $\vec{c}_i$ such that

$$\boldsymbol{R}\left(\theta_i\right)_{y_i} = \begin{bmatrix} \cos\left(\theta_i\right) & 0 & -\sin\left(\theta_i\right) \\ 0 & 1 & 0 \\ \sin\left(\theta_i\right) & 0 & \cos\left(\theta_i\right) \end{bmatrix} \tag{60}$$

$$\boldsymbol{R}\left(\psi_i\right)_{z_i} = \begin{bmatrix} \cos\left(\psi_i\right) & -\sin\left(\psi_i\right) & 0 \\ \sin\left(\psi_i\right) & \cos\left(\psi_i\right) & 0 \\ 0 & 0 & 1 \end{bmatrix}. \tag{61}$$

Let define $C_i = \left[x_{c,i}, y_{c,i}, z_{c,i}\right]^T_{\mathcal{R}}$ the center of $\mathcal{E}_i$ expressed in $\mathcal{R}$ such that

$$C_i = \frac{F_{1,i}\vec{F}_{2,i}}{2} + F_{1,i}. \tag{62}$$

To pass from the referential $\mathcal{R}_i$ to $\mathcal{R}$, let first define the intermediate frame of reference $\mathcal{R}_i^{(2)}$ where $\mathcal{R}_i^{(2)}$ is a translation of referential $\mathcal{R}$ such that its origin is center in C_i. One can get $X_{\mathcal{R}_i^{(2)}}$ in $\mathcal{R}_i^{(2)}$ from $X_{\mathcal{R}_i}$, $\boldsymbol{R}\left(\theta_i\right)_{y_i}$ and $\boldsymbol{R}\left(\psi_i\right)_{z_i}$ such that

$$\begin{aligned} X_{\mathcal{R}_i^{(2)}} &= \boldsymbol{R}\left(\psi_i\right)_z \boldsymbol{R}\left(\theta_i\right)_y X_{\mathcal{R}_i} \\ &= \begin{bmatrix} \cos\left(\theta_i\right)\cos\left(\psi_i\right) & -\sin\left(\psi_i\right) & -\sin\left(\theta_i\right)\cos\left(\psi_i\right) \\ \cos\left(\theta_i\right)\sin\left(\psi_i\right) & \cos\left(\psi_i\right) & -\sin\left(\theta_i\right)\sin\left(\psi_i\right) \\ \sin\left(\theta_i\right) & 0 & \cos\left(\theta_i\right) \end{bmatrix} \\ &\times \begin{bmatrix} x_{\mathcal{R}_i} \\ y_{\mathcal{R}_i} \\ z_{\mathcal{R}_i} \end{bmatrix} \end{aligned} \tag{63}$$

and X in $\mathcal{R}$ can be obtained with $X = X_{\mathcal{R}_i^{(2)}} + C_i$.

Let's find now an expression of $\mathcal{E}_i$ in $\mathcal{R}$. In the same way that (63) provides $X_{\mathcal{R}_i^{(2)}}$ from $X_{\mathcal{R}_i}$, on can get $X_{\mathcal{R}_i}$ from $X_{\mathcal{R}_i^{(2)}}$ using the opposite transformation

$$\begin{aligned} X_{\mathcal{R}_i} &= \text{inv}\left(\boldsymbol{R}\left(-\psi_i\right)_{z_i} \boldsymbol{R}\left(-\theta_i\right)_{y_i}\right) X_{\mathcal{R}_i^{(2)}} \\ &= \boldsymbol{M_c}^i \left(X - C_i\right) \end{aligned} \tag{64}$$

where $\boldsymbol{M_c}^i = \begin{bmatrix} d & e & f \\ g & h & i \\ j & k & l \end{bmatrix}$ with

$$d = \cos\left(\theta_i\right)\cos\left(\psi_i\right) \tag{65}$$
$$e = \cos\left(\theta_i\right)\sin\left(\psi_i\right) \tag{66}$$
$$f = \sin\left(\theta_i\right) \tag{67}$$
$$g = -\sin\left(\psi_i\right) \tag{68}$$
$$h = \cos\left(\psi_i\right) \tag{69}$$
$$i = 0 \tag{70}$$
$$j = -\sin\left(\theta_i\right)\cos\left(\psi_i\right) \tag{71}$$
$$k = -\sin\left(\theta_i\right)\sin\left(\psi_i\right) \tag{72}$$
$$l = \cos\left(\theta_i\right) \tag{73}$$

Evaluation of matrices $\boldsymbol{M_a}$ *and* $\boldsymbol{M_b}$ Consider first $C_i = 0_{3\times1}$, so $\mathcal{R}_i^{(2)} = \mathcal{R}$. Based on (64), one has

$$\begin{cases} x^2_{\mathcal{R}_i} = & (xd + ye + zf)^2 \\ y^2_{\mathcal{R}_i} = & (xg + yh + zi)^2 \\ z^2_{\mathcal{R}_i} = & (xj + yk + zl)^2 \end{cases}$$

$$\begin{cases} x^2_{\mathcal{R}_i} = & x^2d^2 + y^2e^2 + z^2f^2 \\ & +2xyde + 2xzdf + 2yzef \\ y^2_{\mathcal{R}_i} = & x^2g^2 + y^2h^2 + z^2i^2 \\ & +2xygh + 2xzgi + 2yzhi \\ z^2_{\mathcal{R}_i} = & x^2j^2 + y^2k^2 + z^2l^2 \\ & +2xyjk + 2xzjl + 2yzkl \end{cases} \tag{74}$$

Injecting (74) inside (57), one gets

$$\frac{x_{\mathcal{R}_i}^2}{a^2}+\frac{y_{\mathcal{R}_i}^2}{b^2}+\frac{z_{\mathcal{R}_i}^2}{c^2}=1 \tag{75}$$

$$\begin{aligned}&x^2\left(\frac{d^2}{a_i^2}+\frac{g^2}{b_i^2}+\frac{j^2}{c_i^2}\right)+y^2\left(\frac{e^2}{a_i^2}+\frac{h^2}{b_i^2}+\frac{k^2}{c_i^2}\right)\\&+z^2\left(\frac{f^2}{a_i^2}+\frac{i^2}{b_i^2}+\frac{l^2}{c_i^2}\right)+2xy\left(\frac{de}{a_i^2}+\frac{gh}{b_i^2}+\frac{jk}{c_i^2}\right)\\&+2xz\left(\frac{df}{a_i^2}+\frac{gi}{b_i^2}+\frac{jl}{c_i^2}\right)+2yz\left(\frac{ef}{a_i^2}+\frac{hi}{b_i^2}+\frac{kl}{c_i^2}\right)=1\end{aligned} \tag{76}$$

$$x^2\boldsymbol{A}+y^2\boldsymbol{B}+z^2\boldsymbol{C}+2xy\boldsymbol{D}+2xz\boldsymbol{E}+2yz\boldsymbol{F}=1 \tag{77}$$

with

$$\boldsymbol{A}=\frac{d^2}{a_i^2}+\frac{g^2}{b_i^2}+\frac{j^2}{c_i^2} \tag{78}$$

$$\boldsymbol{B}=\frac{e^2}{a_i^2}+\frac{h^2}{b_i^2}+\frac{k^2}{c_i^2} \tag{79}$$

$$\boldsymbol{C}=\frac{f^2}{a_i^2}+\frac{i^2}{b_i^2}+\frac{l^2}{c_i^2} \tag{80}$$

$$\boldsymbol{D}=\frac{de}{a_i^2}+\frac{gh}{b_i^2}+\frac{jk}{c_i^2} \tag{81}$$

$$\boldsymbol{E}=\frac{df}{a_i^2}+\frac{gi}{b_i^2}+\frac{jl}{c_i^2} \tag{82}$$

$$\boldsymbol{F}=\frac{ef}{a_i^2}+\frac{hi}{b_i^2}+\frac{kl}{c_i^2} \tag{83}$$

The equation (77) can be rewritten as

$$0=\bar{X}^T\boldsymbol{M_a}\bar{X} \tag{84}$$

where $\bar{X}=\begin{bmatrix} x & y & z & 1\end{bmatrix}^T$ and

$$\boldsymbol{M_a}=\begin{bmatrix}\boldsymbol{A} & \boldsymbol{D} & \boldsymbol{E} & 0\\ \boldsymbol{D} & \boldsymbol{B} & \boldsymbol{F} & 0\\ \boldsymbol{E} & \boldsymbol{F} & \boldsymbol{C} & 0\\ 0 & 0 & 0 & -1\end{bmatrix}. \tag{85}$$

(77) and (84) are the general expression of $\mathcal{E}_i$ in $\mathcal{R}_i^{(2)}$. To obtain the general expression of $\mathcal{E}_i$ in $\mathcal{R}$, we must add the translation of the center C_i of $\mathcal{E}_i$. This translation can be accomplished using the matrix

$$\boldsymbol{T}=\begin{bmatrix}1 & 0 & 0 & 0\\ 0 & 1 & 0 & 0\\ 0 & 0 & 1 & 0\\ -x_c^i & -y_c^i & -z_c^i & 1\end{bmatrix} \tag{86}$$

such that

$$0=\bar{X}^T\boldsymbol{T}\boldsymbol{M_a}\boldsymbol{T}^T\bar{X} \tag{87}$$

with $\bar{X}=\begin{bmatrix} x & y & z & 1\end{bmatrix}^T$. We note $\boldsymbol{M_b}=\boldsymbol{T}\boldsymbol{M_a}\boldsymbol{T}^T$.

B.2. Proof Definition 3

Let's show the tether i is include inside the ellipsoid of revolution $\mathcal{E}_i$ as defined in Definitions 1 and 2.

The tether is a cable attached in two points: O_i and R_i. Based on the gardener's method, it can be shown a cable can drawn an ellipse corresponding to the maximum distances it can reach, where the two stakes are here O_i and R_i. In three dimensions, this ellipse becomes an ellipsoid of revolution named $\mathcal{E}_i$. Thus, one can observe that O_i and R_i are the two focal of $\mathcal{E}_i$ such that $F_1 = O_i$ and $F_2 = R_i$. This ellipsoid $\mathcal{E}_i$ can be expressed using the parameters defined in Definition 1 and 2, and so θ_i and ψ_i can be evaluated using (6) and (7) using $F_1 = O_i$ and $F_2 = R_i$. One also has $d_i = \left\|F_1F_2\right\| = \left\|O_iR_i\right\|$ the distance between the two focal.

Let's find now the other parameters a_i,b_i and c_i of $\mathcal{E}_i$. First, since $\mathcal{E}_i$ is an ellipsoid of revolution, one has $b_i = c_i$ and so we can study a_i and b_i in the plane with an ellipse. In the following section, parameters used for the demonstration are illustrated on Figure 15.

Let's studied first $b_i = \left\|C_iB\right\|$ with C_i the center of the ellipse. As illustrated in the top subfigure of Figure 15, when the tether is stretched to the point B, it forms two rectangular triangles C_iO_iB and CRB. One has $\left\|O_iC_i\right\| = \frac{\left\|O_iR_i\right\|}{2} = \frac{d_i}{2}$ and $\left\|O_iB\right\| = \frac{L_i}{2}$ because the half of the tether's length L_i. Using Pythagoras theorem, one gets $b_i = \sqrt{\left\|O_iB\right\|^2-\left\|O_iC_i\right\|^2} = \sqrt{\left(\frac{L_i}{2}\right)^2-\left(\frac{d_i}{2}\right)^2}$.

Let's studied now $a_i = \|AC\|$. As illustrated in the bottom subfigure of Figure 15, when the tether is stretched to the point A, one has $L_i = \left\|R_iA\right\| + \left\|A_iO_i\right\| = d_i + 2\bar{a}_i$. Moreover, one has $a_i = \left\|AC_i\right\| = \frac{d_i}{2} + \bar{a}_i$. Thus, one get $\bar{a}_i = a_i - \frac{d_i}{2}$ and so

$$\begin{aligned}L_i &= d_i + 2\bar{a}_i\\ L_i &= d_i + 2\left(a_i - \frac{d_i}{2}\right)\\ a_i &= \frac{L_i}{2}.\end{aligned} \tag{88}$$

B.3. Proof of Theorem 5

We desire to know if between two known instants t_k and t_{k+1} there exist an instant $t \in \left[t_k, t_{k+1}\right]$ such that the segment $\left[O_iR_i\right](t)$ and the segment $\left[O_jR_j\right](t)$ are intersecting, *i.e.* $\exists t_{colli} \in \left[t_k, t_{k+1}\right]$ such that $\left[O_iR_i\right]\left(t_{colli}\right) \cap \left[O_jR_j\right]\left(t_{colli}\right) \neq \emptyset$. We consider in this proof that the system is discrete, so there is very few chance that the instant t_{colli} corresponds to an instant t_k and can therefore be evaluated numerically: another way to detect the intersection must be found.

Let's first define $\bar{S}_i(t) \in \left[O_iR_i\right](t)$ and $\bar{S}_j(t) \in \left[O_jR_j\right](t)$ the closest points between the two main axis between the ellipsoid $\mathcal{E}_i^L(t)$ and $\mathcal{E}_j^L(t)$ (Theorem 10 in Appendix A.1 proposes a method to evaluate these points). Let define the vector $\vec{v_{ij}}(t) = \bar{S}_j(t) - \bar{S}_i(t)$.

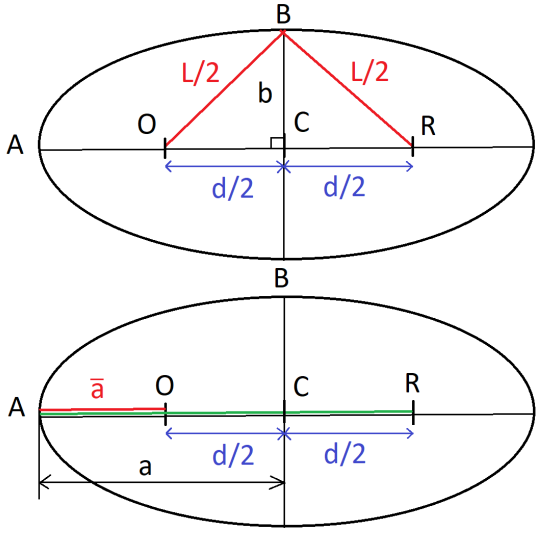

Figure 15: Ellipsoid parameters used for the proof.

Suppose there is an intersection between t_k and t_{k+1}. For $t \in [t_k, t_{colli}]$, the distance $\left\|\bar{S}_j\bar{S}_i\right\|(t)$ reduces since becoming equal to zero. For $t \in [t_{colli}, t_{k+1}]$, the distance $\left\|\bar{S}_j\bar{S}_i\right\|(t)$ grows from zero to $\left\|\bar{S}_j\bar{S}_i\right\|(t_{k+1})$. However, between t^-_{colli} and t^+_{colli}, the direction of vector $\vec{v_{ij}}(t)$ switches to its opposite direction. Thus, one has $\vec{v_{ij}}(t^-_{colli}).\vec{v_{ij}}(t^+_{colli}) \leq 0$. Then, if t_k and t_{k+1} induces a small displacement, *i.e.* $\left|\left\|\vec{v_{ij}}(t_k)\right\| - \left\|\vec{v_{ij}}(t_{k+1})\right\|\right| < \varepsilon$ with $\varepsilon > 0$ relatively small, then one has $\vec{v_{ij}}(t_k).\vec{v_{ij}}(t_{k+1}) \leq 0$.

B.4. Prove for theorems with closest points between two lines and segments

B.4.1. Closest points between two lines

Let define two lines (O_1R_1) and (O_2R_2) where O_1, R_1, O_2 and R_2 are points with coordinate expressed in $\mathcal{R}$. A point $P_1 \in (O_1R_1)$ on the line (O_1R_1) can be expressed as

$$P_1 = t_1\vec{V}_1 + O_1 \tag{89}$$
$$\vec{V}_1 = R_1 - O_1 \tag{90}$$

where $t_1 \in]-\infty, \infty[$ for a line (O_1R_1) and $t_1 \in [0, 1]$ for the segment $[O_1R_1]$. Similarly for a point P_2 on line (O_2R_2) with parameters t_2 and $\vec{V}_2$. Suppose the two lines are not parallel, *i.e.* $\frac{\left|\vec{V}_2.\vec{V}_1\right|}{\left\|\vec{V}_2\right\|\left\|\vec{V}_1\right\|} \neq 1$.

The idea is that the shortest segment between two lines must be perpendicular to the other lines. Let (P_1P_3) be the perpendicular line starting from a point P_1 of the first line and let define P_3 such that

$$P_3 = t_3\vec{V}_3 + P_1 \tag{91}$$

where $t_3 \in]-\infty, \infty[$ and with $\vec{V}_3 = \vec{V}_2 \wedge \vec{V}_1$, *i.e.* $\vec{V}_3.\vec{V}_2 = 0$ and $\vec{V}_3.\vec{V}_1 = 0$. Then, for this line (P_1P_3) meets also the second line (O_2R_2), we need that P_2 coincide with P_3:

$$\begin{aligned} P_3 &= P_2 \\ t_3\vec{V}_3 + P_1 &= t_2\vec{V}_2 + O_2 \\ t_3\vec{V}_3 + (t_1V_1 + O_1) &= t_2\vec{V}_2 + O_2 \\ t_3\vec{V}_3 - t_2\vec{V}_2 + t_1\vec{V}_1 &= O_2 - O_1 \end{aligned} \tag{92}$$

We have t_1, t_2 and t_3 the unknown parameters, which can be obtained by solving the system

$$S3 = \begin{cases} t_3v_{x3} - t_2v_{x2} + t_1v_{x1} &= x_{O,2} - x_{O,1} \\ t_3v_{y3} - t_2v_{y2} + t_1v_{y1} &= y_{O,2} - y_{O,1} \\ t_3v_{z3} - t_2v_{z2} + t_1v_{z1} &= z_{O,2} - z_{O,1} \end{cases} \tag{93}$$

where for $i \in [1, 2, 3]$, $\vec{V}_i = \begin{bmatrix} v_{x,i} & v_{y,i} & v_{z,i} \end{bmatrix}^T$ and $O_i = \begin{bmatrix} x_{O,i} & y_{O,i} & z_{O,i} \end{bmatrix}^T$.

By solving the system (93) (resolution may depend of presence of potential elements equal to zero), one can express the two closest points Q_1 and Q_2 of the lines (O_1R_1) and (O_2R_2) as

$$Q_1 = O_1 + t_1\vec{V}_1, \tag{94}$$
$$Q_2 = O_2 + t_2\vec{V}_2. \tag{95}$$

B.4.2. Closest points between a point and line or segment

Following the same idea than in Appendix B.4.1, we search the vector $\vec{S_1P_2}$ orthogonal to $\vec{V}_1$. Since S_1 can be expressed as $S_1 = O_1 + t_1\vec{V}_1$ with $t_1 \in \mathbb{R}$, one gets

$$\begin{aligned} \vec{V}_1.\vec{S_1P_2} &= 0 \\ \vec{V}_1.(P_2 - S_1) &= 0 \\ \vec{V}_1.\left(P_2 - \left(O_1 + t_1\vec{V}_1\right)\right) &= 0 \\ \vec{V}_1.P_2 - t_1\left\|\vec{V}_1\right\|^2 - \vec{V}_1.O_1 &= 0 \end{aligned}$$

$$t_1 = \frac{\vec{V}_1.P_2 - \vec{V}_1.O_1}{\left\|\vec{V}_1\right\|^2} \tag{96}$$

and so

$$S_1 = O_1 + t_1\vec{V}_1 \tag{97}$$

is the closest point of P_2 on the line (O_1R_1).

Let's check now if this point S_1 is on the segment $[O_1R_1]$. Using Definition 9, one has

$$\bar{S}_1 = \begin{cases} R_1 & \text{if } (\|S_1O_1\| > \|O_1R_1\|) \,\&\, (\|S_1O_1\| > \|S_1R_1\|) \\ O_1 & \text{if } (\|S_1R_1\| > \|O_1R_1\|) \,\&\, (\|S_1O_1\| < \|S_1R_1\|) \\ S_1 & \text{else.} \end{cases} \tag{98}$$

B.4.3. Closest points between two segments

Let define the two segments $[O_1R_1]$ and $[O_2R_2]$. We note $\bar{S}_1 \in [O_1R_1]$ and $\bar{S}_2 \in [O_2R_2]$ the two closest points between $[O_1R_1]$ and $[O_2R_2]$.

Particular case: $O_1 = R_1$ and/or $O_2 = R_2$ Suppose first that $O_1 = R_1$ and $O_2 = R_2$. Then the two closest points are $\bar{S}_1 = O_1$ and $\bar{S}_2 = O_2$.

Suppose now that one of the two segments is a point, *i.e.* $O_2 = R_2$. Then $\bar{S}_2 = O_2$ and we can found $\bar{S}_1$ using Theorem 9. Similarly if $O_1 = R_1$.

General case: $O_1 \neq R_1$ and $O_2 \neq R_2$ Suppose here that $O_1 \neq R_1$ and $O_2 \neq R_2$. Consider also $Q_1$and Q_2 the closest points between the two lines (O_1R_1) and (O_2R_2) as defined in Theorem 8 and evaluated in Appendix B.4.3.

To find $\bar{S}_1$ and $\bar{S}_2$, let's first evaluate $Q_1$and Q_2 and consider the following cases:

1. If $Q_1 \in [O_1R_1]$ and $Q_2 \in [O_2R_2]$, *i.e.* Q_1 and Q_2 are respectively on the segment $[O_1R_1]$ and $[O_2R_2]$, then one has $\bar{S}_1 = Q_1$ and $\bar{S}_2 = Q_2$.
2. If $Q_1 \notin [O_1R_1]$ or $Q_2 \notin [O_2R_2]$, one or both of $\bar{S}_1$ and $\bar{S}_2$ is an extremity of segments $[O_1R_1]$ and $[O_2R_2]$. We must perform the following tests to check it.

Note that the test $Q_1 \in [O_1R_1]$ and $Q_2 \in [O_2R_2]$ can be performed using Definition 9.

To find the solution in the second case, we must evaluate

1. the closest point $\bar{S}_2^{(2)} \in [O_2R_2]$ of the line (O_1R_1) and then the closest point$\bar{S}_1^{(2)} \in [O_1R_1]$ of $\bar{S}_2^{(2)}$,
2. the closest point $\bar{S}_1^{(1)} \in [O_1R_1]$ of the line (O_2R_2) and then the closest point$\bar{S}_2^{(1)} \in [O_2R_2]$ of $\bar{S}_1^{(1)}$,
3. Compare the distance $\left\|\bar{S}_1^{(1)}\bar{S}_2^{(1)}\right\|$ and $\left\|\bar{S}_1^{(2)}\bar{S}_2^{(2)}\right\|$ to find the couple of solution corresponding to the shortest distance.

Following section described the details of steps described above.

Consider first Q_2. Based on Definition 9, the closest point $\bar{S}_2^{(2)}$ of the segment $[O_1R_1]$ can be expressed as

$$\bar{S}_2^{(2)} = \begin{cases} R_2 & \text{if } \left(\|Q_2O_2\| > \|O_2R_2\|\right) \,\&\, \left(\|Q_2O_2\| > \|Q_2R_2\|\right) \\ O_2 & \text{if } \left(\|Q_2R_2\| > \|O_2R_2\|\right) \,\&\, \left(\|Q_2O_2\| < \|Q_2R_2\|\right) \\ Q_2 & \text{else} \end{cases} \tag{99}$$

Using Theorem 9, one gets $\bar{S}_1^{(2)} \in [O_1R_1]$ the closest point of $\bar{S}_2^{(2)}$ to get the couple of solution $\left(\bar{S}_1^{(2)}, \bar{S}_2^{(2)}\right)$.

Consider now Q_1. Following the same calculation, one can get a second couple of solution $\left(\bar{S}_1^{(1)}, \bar{S}_2^{(1)}\right)$.

We can now evaluate the distance $\left\|\bar{S}_1^{(1)}\bar{S}_2^{(1)}\right\|$ and $\left\|\bar{S}_1^{(2)}\bar{S}_2^{(2)}\right\|$ to find the solution of our problem:

$$\left(\bar{S}_1, \bar{S}_2\right) = \begin{cases} \left(\bar{S}_1^{(1)}, \bar{S}_2^{(1)}\right) & \text{if } \left\|\bar{S}_1^{(1)}\bar{S}_2^{(1)}\right\| < \left\|\bar{S}_1^{(2)}\bar{S}_2^{(2)}\right\| \\ \left(\bar{S}_1^{(2)}, \bar{S}_2^{(2)}\right) & \text{else.} \end{cases} \tag{100}$$

B.5. Proof intersection plane and ellipsoid

Consider a plane $\mathcal{P}$ as expressed in Definition 5 and an ellipsoid of revolution $\mathcal{E}_i$ as defined in Definition 2. The intersection between $\mathcal{P}$ and $\mathcal{E}_i$ is an ellipse: if this ellipse exists, then there is a collision between $\mathcal{P}$ and $\mathcal{E}_i$. Let's find the expression of the ellipse.

In the ellipsoid referential $\mathcal{R}_i = \left(C_i, \vec{a_i}, \vec{b_i}, \vec{c_i}\right)$, $\mathcal{E}_i$ can be expressed as

$$\frac{x^2}{a^2} + \frac{y^2}{b^2} + \frac{z^2}{c^2} = 1 \tag{101}$$

In the same way, based on Definition 1 and Definition 5, the plane $\mathcal{P}\left(P, \vec{n}\right)$ can be expressed in $\mathcal{R}_i$ such as

$$\bar{\alpha}x + \bar{\beta}y + \bar{\gamma}z + \bar{\delta} = 0 \tag{102}$$

$$\bar{\delta} = -\left(\bar{\alpha}\bar{x}_P + \bar{\beta}\bar{y}_P + \bar{\gamma}\bar{z}_P\right) \tag{103}$$

with $\vec{\bar{n}} = \begin{bmatrix} \bar{\alpha} & \bar{\beta} & \bar{\gamma} \end{bmatrix}^T$ *and* $P = \left[\bar{x}_P, \bar{y}_P, \bar{z}_P\right]^T$ *expressed as*

$$\bar{P}_{\mathcal{R}_i} = \boldsymbol{M_c}^i \left(P - C_{i|\mathcal{R}}\right) \tag{104}$$

$$\vec{\bar{n}}_{\mathcal{R}_i} = \boldsymbol{M_c}^i \vec{n}_{\mathcal{R}} \tag{105}$$

with $\boldsymbol{M_c}^i$ associated to $\mathcal{E}_i$ as defined in Definition 2.

Consider first that $\bar{\gamma} \neq 0$. From (102), one gets $z = -\left(\frac{\bar{\alpha}}{\bar{\gamma}}x + \frac{\bar{\beta}}{\bar{\gamma}}y + \frac{\bar{\delta}}{\bar{\gamma}}\right)$ and so

$$\begin{aligned} z^2 &= \left(\frac{\bar{\alpha}}{\bar{\gamma}}x + \frac{\bar{\beta}}{\bar{\gamma}}y + \frac{\bar{\delta}}{\bar{\gamma}}\right)^2 \\ &= \left(\frac{\bar{\alpha}}{\bar{\gamma}}\right)^2 x^2 + \left(\frac{\bar{\beta}}{\bar{\gamma}}\right)^2 y^2 + \left(\frac{\bar{\delta}}{\bar{\gamma}}\right)^2 \\ &\quad + 2\frac{\bar{\alpha}\bar{\beta}}{\bar{\gamma}^2}xy + 2\frac{\bar{\alpha}\bar{\delta}}{\bar{\gamma}^2}x + 2\frac{\bar{\beta}\bar{\delta}}{\bar{\gamma}^2}y. \end{aligned} \tag{106}$$

Injecting (106) in (101), one gets

$$\begin{aligned} \frac{x^2}{a^2} + \frac{y^2}{b^2} + \frac{\left(\frac{\bar{\alpha}}{\bar{\gamma}}x + \frac{\bar{\beta}}{\bar{\gamma}}y + \frac{\bar{\delta}}{\bar{\gamma}}\right)^2}{c^2} - 1 = 0 \\ \left(\frac{\bar{\alpha}^2}{\bar{\gamma}^2} + \frac{c^2}{a^2}\right)x^2 + \left(\frac{\bar{\beta}^2}{\bar{\gamma}^2} + \frac{c^2}{b^2}\right)y^2 + \left(\frac{\bar{\delta}^2}{\bar{\gamma}^2} - c^2\right) \\ +2\frac{\bar{\alpha}\bar{\beta}}{\bar{\gamma}^2}xy + 2\frac{\bar{\alpha}\bar{\delta}}{\bar{\gamma}^2}x + 2\frac{\bar{\beta}\bar{\delta}}{\bar{\gamma}^2}y = 0 \end{aligned}$$

$$A_0x^2 + 2B_0xy + C_0y^2 + 2D_0x + 2E_0y + F_0 = 0 \tag{107}$$

with

$$\begin{aligned} A_0 &= \frac{\bar{\alpha}^2}{\bar{\gamma}^2} + \frac{c^2}{a^2} \quad & B_0 &= \frac{\bar{\alpha}\bar{\beta}}{\bar{\gamma}^2} \\ C_0 &= \frac{\bar{\beta}^2}{\bar{\gamma}^2} + \frac{c^2}{b^2} \quad & D_0 &= \frac{\bar{\alpha}\bar{\delta}}{\bar{\gamma}^2} \\ E_0 &= \frac{\bar{\beta}\bar{\delta}}{\bar{\gamma}^2} \quad & F_0 &= \frac{\bar{\delta}^2}{\bar{\gamma}^2} - c^2 \end{aligned}$$

(107) is the equation of the intersection between $\mathcal{P}$ and $\mathcal{E}_i$, which is a conic equation. If there is an intersection, then (107) is the equation of an ellipse. Finally (107) is the equation of an ellipse if

$$\left(T_1 > 0\right) \,\&\, \left(T_2 > 0\right) \tag{108}$$

where

$$T_1 = A_0C_0 - B_0^2 \tag{109}$$

$$T_2 = \left(B_0D_0 - A_0E_0\right)^2 - \left(D_0^2 - A_0F_0\right)\left(B_0^2 - A_0C_0\right). \tag{110}$$

The detail of this condition can be found here[1] .

B.6. Proof of Theorem 12

Consider a tether system $\mathcal{S}_i$ with an target position R_i^* and an ellipsoid obstacle $\mathcal{E}_{\text{obs}}$ as defined in Definition 2, with $d_{\text{obs}} = \left[F_{1,\text{obs}}F_{2,\text{obs}}\right]$ the vector of the main axis. $\mathcal{E}_{\text{obs}}$ is considered on the path of $\mathcal{S}_i$ if its main axis d_{obs} will have to intersect with the main axis d_i of $\mathcal{E}_i^L \in \mathcal{S}_i$.

Consider a plane $\mathcal{P}_k$ containing the triangle $O_iR_iP_i$. The intersection between $\mathcal{P}$ and the line $\left(F_{1,\text{obs}}F_{2,\text{obs}}\right)$ is an point P_a: one must check first if P_a is on the segment $F_{1,\text{obs}}F_{2,\text{obs}}$, then check if P_a is inside the triangle $O_iR_iR_i^*$.

The plane $\mathcal{P}_k\left(\vec{n}_k, P_k\right)$ which contain the triangle $O_iR_iP_i$ can be expressed following Definition 5 with $\vec{n}_k = \vec{O_iR_i} \wedge \vec{O_iR_i^*}$ and $P_k = O_i$. One can deduce α_k, β_k, γ_k such that $\vec{n}_k = \begin{bmatrix} \alpha_k & \beta_k & \gamma_k \end{bmatrix}^T$ and $\delta_k = -\left(\alpha_k x_{O,i} + \beta_k y_{O,i} + \gamma_k z_{O,i}\right)$. A point P on the line $\left(F_{1,\text{obs}}F_{2,\text{obs}}\right)$ can be expressed as

$$P = F_{1,\text{obs}} + t\vec{V}_{\text{obs}} \tag{111}$$

where $\vec{V}_{\text{obs}} = \vec{F_{1,\text{obs}}F_{2,\text{obs}}} = \begin{bmatrix} v_x & v_y & v_z \end{bmatrix}$ and $t \in \mathbb{R}$. If $\vec{V}_{\text{obs}}$ and $\vec{n}_k$ are not orthogonal, *i.e.* $\vec{V}_{\text{obs}}.\vec{n}_k \neq 0$, the intersection $P_a = \begin{bmatrix} x_a & y_a & z_a \end{bmatrix}^T$ between $\left(F_{1,\text{obs}}F_{2,\text{obs}}\right)$ and $\mathcal{P}_k$ is the solution of the following system

$$\begin{cases} tv_x + x_{F_{1,\text{obs}}} &= x_a \\ tv_y + y_{F_{1,\text{obs}}} &= y_a \\ tv_z + z_{F_{1,\text{obs}}} &= z_a \\ \alpha_k x_a + \beta_k y_a + \gamma_k z_a &= 0 \end{cases} \tag{112}$$

[1] https://www.imo.universite-paris-saclay.fr/~daniel.perrin/CAPES/geometrie/ellipses.pdf

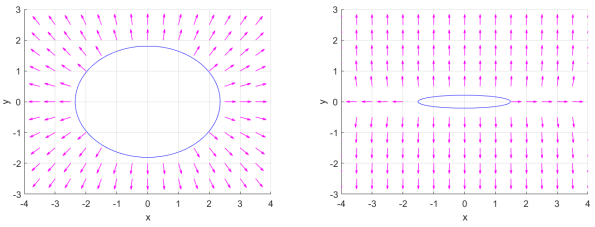

Figure 16: Repulsive vector $\vec{v}_1$ if it was generate using the Jacobian of $\mathcal{E}_j$. Left: $b_j = c_j = 0.8a_j$. Right: $b_j = c_j = 0.13a_j$

with $F_{1,\text{obs}} = \begin{bmatrix} x_{F_{1,\text{obs}}} & y_{F_{1,\text{obs}}} & z_{F_{1,\text{obs}}} \end{bmatrix}^T$ and where x_a, y_a, z_a and t are the unknown variables.

Then, one must check if $P_a \in \left[F_{1,\text{obs}}F_{2,\text{obs}}\right]$ using for example Definition 9. If $P_a \notin \left[F_{1,\text{obs}}F_{2,\text{obs}}\right]$, main axis $d_{\text{obs}}$of $\mathcal{E}_{\text{obs}}$ does not intersect with plane $\mathcal{P}_k$ and so $\mathcal{E}_{\text{obs}}$ is not on the path between R_i and its target R_i^*.

If $P_a \in \left[F_{1,\text{obs}}F_{2,\text{obs}}\right]$, let's check if P_a is inside the triangle $O_iR_iR_i^*$. The point P_a is inside the triangle $O_iR_iR_i^*$ if the sum of the area of $O_iR_iP_a$, $O_iR_i^*P_a$ and $R_iR_i^*P_a$ is equal to the area of the triangle $O_iR_iR_i^*$. Let's note $\mathcal{A}_{ABC}$ the area of a triangle ABC and one has

$$\mathcal{A}_{ABC} = \frac{\left\|\vec{AB} \wedge \vec{AC}\right\|}{2}. \tag{113}$$

So if one has $T_3 = 0$ with $T_3 = \mathcal{A}_{O_iR_iR_i^*} - \left(\mathcal{A}_{O_iR_iP_a} + \mathcal{A}_{O_iP_aR_i^*} + \mathcal{A}_{P_aR_iR_i^*}\right)$, then P_a is inside the triangle $O_iR_iR_i^*$, and so $\mathcal{E}_{\text{obs}}$ is on the path between R_i and its target R_i^*. Else if $T_3 \neq 0$, $\mathcal{E}_{\text{obs}}$ is not on the path.

B.7. Calculation of vectors $\vec{v}_1$, $\vec{v}_2$ and $\vec{v}_3$

B.7.1. Choice of the repulsive field

The first idea to create the repulsive force $\vec{v}_1$ was to use the Jacobian matrix$\mathcal{E}_j$.While it offers an interesting repulsion when the axes of the ellipsoid are more or less equal, the repulsion created when the ellipsoid is flat makes it more difficult for the ROV to go around the ellipsoid near its extremities, as illustrated in Figure 16. Therefore, we preferred to create our own repulsive field, which makes it easier to get around the extremities of the ellipsoid while pushing the ROV away from them. Moreover, the proposed form is more adapted to bypass system $\mathcal{S}_j$ which combine several ellipsoids.

B.7.2. Description of calculation of $\vec{v}_1$

Consider first $\vec{v}_0 = \vec{C_jR_i} = R_i - C_j$ the vector between the center of $\mathcal{E}_j$ and the ROV R_i. Let's also define $\vec{v}_{d_j} = \frac{\vec{d}_j}{\left\|\vec{d}_j\right\|}$ the unitary vector of the main axis $\mathcal{E}_j$. Let's define E_j and $\bar{E}_j$ the nearest and farthest focal of $\mathcal{E}_j$ from R_i such as

$$E_j = \begin{cases} F_{1,j} & \text{if } \left\|R_iF_{1,j}\right\| < \left\|R_iF_{2,j}\right\| \\ F_{2,j} & \text{else} \end{cases} \tag{114}$$

$$\bar{E}_j = \begin{cases} F_{2,j} & \text{if } \left\|R_i F_{1,j}\right\| < \left\|R_i F_{2,j}\right\| \\ F_{1,j} & \text{else} \end{cases} \tag{115}$$

and let define $\vec{v}_{12} = R_i - E_j$ and $\vec{v}_{13} = R_i - \bar{E}_j$.

Let's define H the projection of R_i on the line $\left(F_{1,j}F_{2,j}\right)$ (of axis $\vec{d}_j$) without need to calculate it. If $\left|\vec{v}_{d_j}.\vec{v}_{13}\right| > d_j$, then H is not on the segment $\left[F_{1,j}F_{2,j}\right]$. To create the potential field $\vec{v}_1$ illustrated in Figure 16, three cases must be considered: if $H \in \left[F_{1,j}F_{2,j}\right]$, then the ROV R_i is repulsed orthogonality to axis $\vec{d}_j$, which can be expressed with $\vec{v}_{11} = \vec{v}_0 - \vec{v}_{d_j}\left(\vec{v}_{d_j}.\vec{v}_0\right)$. Else, the ROV R_i is repulsed from the closest focal E_j , so in the direction $\vec{v}_{12}$.

One so have

$$\vec{v}_1 = \begin{cases} \vec{v}_{11} & \text{if } H \in \left[F_{1,j}F_{2,j}\right] \\ \vec{v}_{12} & \text{else} \end{cases} \tag{116}$$

which can be rewritten as

$$\vec{v}_1 = \begin{cases} R_i - F_{1,j} & \text{if } \left(\left|\vec{v}_{d_j}.\vec{F_{2,j}R_i}\right| > d_j\right) \\ & \quad \& \left(\left\|R_i F_{1,j}\right\| < \left\|R_i F_{2,j}\right\|\right) \\ R_i - F_{2,j} & \text{if } \left(\left|\vec{v}_{d_j}.\vec{F_{1,j}R_i}\right| > d_j\right) \\ & \quad \& \left(\left\|R_i F_{1,j}\right\| > \left\|R_i F_{2,j}\right\|\right) \\ \vec{v}_{10} & \text{else.} \end{cases} \tag{117}$$

with $\vec{v}_{10} = \vec{C_jR_i} - \vec{v}_{d_j}\left(\vec{v}_{d_j}.\vec{C_jR_i}\right)$.

Finally, we normalized $\vec{v}_1$ if this one is not equal to zero:

$$\vec{v}_1 = \begin{cases} \frac{\vec{v}_1}{\left\|\vec{v}_1\right\|} & \text{if } \left\|\vec{v}_1\right\| \neq 0 \\ 0_{3\times 1} & \text{else.} \end{cases} \tag{118}$$

B.7.3. Description of calculation of $\vec{v}_2$ and $\vec{v}_3$

The two $\vec{v}_2$ and $\vec{v}_3$ are "rotary" forces which help to bypass the obstacle $\mathcal{E}_j$ in direction of the objective $\hat{R}_i^*$. Thus, we desire to create potential field orthogonal to $\vec{v}_1$.

Since $\vec{v}_1$ is orthogonal to $\vec{v}_{d_j}$ when $H \in \left[F_{1,j}F_{2,j}\right]$, let's define the three orthogonal axis $\vec{v}_1$, $\vec{v}_{d_j}$ and $\vec{v}_{30} = \vec{v}_1 \wedge \vec{v}_{d_j}$. To consider the cases at the extremity where $\vec{v}_1$ and $\vec{v}_{d_j}$ are not orthogonal, we introduce $\vec{v}_{20} = \vec{v}_1 \wedge \vec{v}_{30}$ and keep the three vectors $\vec{v}_1$, $\vec{v}_{30}$ and $\vec{v}_{20}$.

$\vec{v}_1$ pushes the ROV R_i away from the ellipsoid $\mathcal{E}_j$, so let's use $\vec{v}_{20}$ and $\vec{v}_{30}$ to lead the rotation around $\mathcal{E}_j$. However, we would like that the rotation leads R_i closer to $\hat{R}_i^*$, so let's check if $\vec{v}_{20}$ and $\vec{v}_{30}$ turn in the right direction.

For $\vec{v}_{20}$, we use $\vec{v}_{30}$ as axis of rotation. Let $\vec{v}_0 = R_i - C_j$ be the orientation of R_i from the center of $\mathcal{E}_j$ and $\vec{v}_4 = \hat{R}_i^* - R_i$ be the shortest direction to the target $\hat{R}_i^*$. We can define the position R_i as a point on the circle C_2 of center C_j, radius $\left\|\vec{v}_0\right\|$ and $\vec{v}_{30}$ as axis of rotation. So we can define $\vec{v}_{\text{rot2}} = s\left(\vec{v}_0 \wedge \vec{v}_{30}\right)$ with $s \in \{-1, 1\}$ the tangents of C_2, and we define the direction s of rotation $\vec{v}_{\text{rot2}}$ such that $\vec{v}_{\text{rot2}}.\vec{v}_4 > 0$, *i.e.* in the shortest direction to the objective. One gets

$$\vec{v}_{\text{rot2}} = \left(\vec{v}_0 \wedge \vec{v}_{30}\right) \text{sign}\left(\left(\vec{v}_0 \wedge \vec{v}_{30}\right).\vec{v}_4\right). \tag{119}$$

We create so $\vec{v}_2$ based on vector $\vec{v}_{20}$ but with the direction of $\vec{v}_{\text{rot2}}$ such that

$$\vec{v}_2 = \begin{cases} \frac{\vec{v}_{20}}{\left\|\vec{v}_{20}\right\|}\text{sign}\left(\vec{v}_{20}.\vec{v}_{\text{rot2}}\right) & \text{if } \left\|\vec{v}_{20}\right\| \neq 0 \\ 0_{3\times 1} & \text{else.} \end{cases} \tag{120}$$

In the same way for $\vec{v}_{30}$, using $\vec{v}_{d_j}$ instead of $\vec{v}_{30}$ as axis of rotation, one gets

$$\vec{v}_{\text{rot3}} = \left(\vec{v}_0 \wedge \vec{v}_{d_j}\right) \text{sign}\left(\left(\vec{v}_0 \wedge \vec{v}_{d_j}\right).\vec{v}_4\right) \tag{121}$$

and so

$$\vec{v}_3 = \begin{cases} \frac{\vec{v}_{30}}{\left\|\vec{v}_{30}\right\|}\text{sign}\left(\vec{v}_{30}.\vec{v}_{\text{rot3}}\right) & \text{if } \left\|\vec{v}_{30}\right\| \neq 0 \\ \vec{0}_3 & \text{else.} \end{cases} \tag{122}$$

Finally, the three forces are combined with the ration $\vec{f}_r^{i,j} = \frac{2\vec{v}_1+\vec{v}_2+\vec{v}_3}{\left\|2\vec{v}_1+\vec{v}_2+\vec{v}_3\right\|}$ such that the action of $\vec{v}_1$ remains dominant over $\vec{v}_2$ and $\vec{v}_3$ since it is $\vec{v}_1$ which guarantee the absence of collision with $\mathcal{E}_j$.

B.8. Proof of Theorem 13

Consider the ellipsoid $\mathcal{E}_{\text{obs}}^{i,j}$ in its own frame $\mathcal{R}_j$ as defined in Definition 1. In $\mathcal{R}_j$, the equation of $\mathcal{E}_{\text{obs}}^{i,j}$ can be expressed as

$$E_1 : \quad \frac{x^2}{a_j^2} + \frac{y^2}{b_j^2} + \frac{z^2}{c_j^2} = 1.$$

Evaluate now the position of $O_{i|\mathcal{R}_j}$, center of the tangent sphere $C_{\text{tangent}}^{i,j}$, in the frame of reference $\mathcal{R}_j$:

$$O_{i|\mathcal{R}_j} = \boldsymbol{M_c}^j\left(O_{i|\mathcal{R}} - C_{j|\mathcal{R}}\right)$$

with $C_{j|\mathcal{R}}$ the center of $\mathcal{E}_{\text{obs}}^{i,j}$. In $\mathcal{R}_j$ the equation of sphere $C_{\text{tangent}}^{i,j}$ can be expressed as

$$E_2 : \quad \left(x - x_c\right)^2 + \left(y - y_c\right)^2 + \left(z - z_c\right)^2 = R^2$$

with $O_{i|\mathcal{R}_j} = \begin{bmatrix} x_c & y_c & z_c \end{bmatrix}_{\mathcal{R}_j}^T$ and R the radius we desire to find.

At the common tangent point of the ellipse and the circle noted $X = \begin{bmatrix} x & y & z \end{bmatrix}^T$, the two volumes share a normal

line $\vec{n}_{ij}$. The vectors normal at point $X = \begin{bmatrix} x & y & z \end{bmatrix}^T$ for $\mathcal{E}^{i,j}_{\text{obs}}$ and $\mathcal{C}^{i,j}_{\text{tangent}}$ are

$$\vec{n}_{E_1} = \begin{bmatrix} \frac{d}{dx}E_1 \\ \frac{d}{dy}E_1 \\ \frac{d}{dz}E_1 \end{bmatrix} = \begin{bmatrix} 2\frac{x}{a_j^2} \\ 2\frac{y}{b_j^2} \\ 2\frac{z}{c_j^2} \end{bmatrix}$$

$$\vec{n}_{E_2} = \begin{bmatrix} \frac{d}{dx}E_2 \\ \frac{d}{dy}E_2 \\ \frac{d}{dz}E_2 \end{bmatrix} = \begin{bmatrix} 2\left(x - x_c\right) \\ 2\left(y - y_c\right) \\ 2\left(z - z_c\right) \end{bmatrix}.$$

A solution to find $\vec{n}_{ij}$ is to solve $\vec{n}_{E_1} \wedge \vec{n}_{E_2} = 0$:

$$\begin{cases} 4\left(y - y_c\right)\frac{z}{c_j^2} - 4\left(z - z_c\right)\frac{y}{b_j^2} = 0 \\ 4\left(z - z_c\right)\frac{x}{a_j^2} - 4\left(x - x_c\right)\frac{z}{c_j^2} = 0 \\ 4\left(x - x_c\right)\frac{y}{b_j^2} - 4\left(y - y_c\right)\frac{x}{a_j^2} = 0 \end{cases}$$

$$\begin{cases} b_j^2\left(y - y_c\right)z - c_j^2\left(z - z_c\right)y &= 0 \\ c_j^2\left(z - z_c\right)x - a_j^2\left(x - x_c\right)z &= 0 \\ a_j^2\left(x - x_c\right)y - b_j^2\left(y - y_c\right)x &= 0 \end{cases} \tag{123}$$

Moreover, X must be on the ellipsoid, so

$$\begin{cases} b_j^2\left(y - y_c\right)z - c_j^2\left(z - z_c\right)y &= 0 \\ c_j^2\left(z - z_c\right)x - a_j^2\left(x - x_c\right)z &= 0 \\ a_j^2\left(x - x_c\right)y - b_j^2\left(y - y_c\right)x &= 0 \\ \frac{x^2}{a_j^2} + \frac{y^2}{b_j^2} + \frac{z^2}{c_j^2} &= 1 \end{cases} \tag{124}$$

We have too many equations to solve the system: we can delete one

$$\begin{cases} b_j^2\left(y - y_c\right)\left(z - z_{c2}\right) - c_j^2\left(z - z_c\right)\left(y - y_{c2}\right) &= 0 \\ c_j^2\left(z - z_c\right)\left(x - x_{c2}\right) - a_j^2\left(x - x_c\right)\left(z - z_{c2}\right) &= 0 \\ \frac{\left(x - x_{c2}\right)^2}{a_j^2} + \frac{\left(y - y_{c2}\right)^2}{b_j^2} + \frac{\left(z - z_{c2}\right)^2}{c_j^2} &= 1 \end{cases} \tag{125}$$

N_s solution can be found from (125): we keep only the real solutions in $S_X = \left\{X_{(k)} \middle| \, k \in \left[1 \dots N_s\right], \, \text{Im}\left(X_{(k)}\right) = 0\right\}$ with $X_{(k)} = \begin{bmatrix} x_{(k)} & y_{(k)} & z_{(k)} \end{bmatrix}$ solution of (125).

Once (123) solved, the radius $R = r^{i,j}_{\text{tangent}}$ can be expressed as

$$r^{i,j}_{\text{tangent}} = \min_{X_{(k)} \in S_X} \left(\sqrt{X_{(k)}^T X_c}\right) \tag{126}$$

with $X_c = O_{i|\mathcal{R}_j} = \begin{bmatrix} x_c & y_c & z_c \end{bmatrix}^T_{\mathcal{R}_j}$.

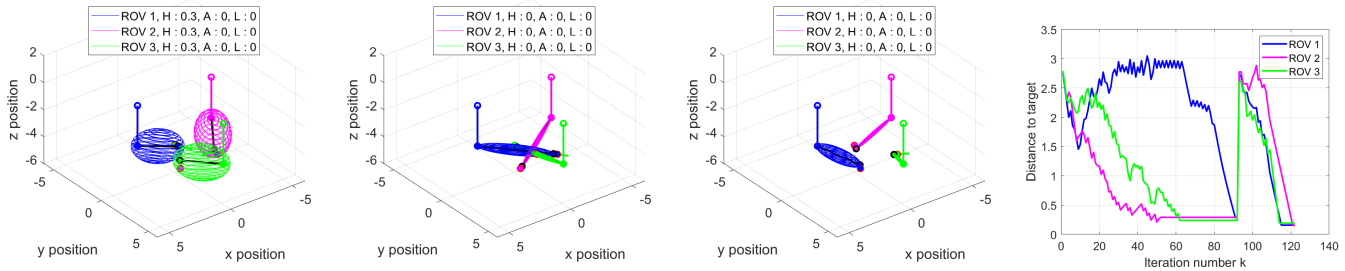

(b) Initial position (c) First target reached (d) Second target reached (e) Distance ROVs to current target

(e) Three ROVs' tethers searching to reach a target to form the bisectors of a triangle, then switch its position to reach the target position of the ROV on its right. Colored ellipsoid represented the tether. Intersection between ellipsoid $\mathcal{E}^L$ are authorized ("ellipsoid obstacle").

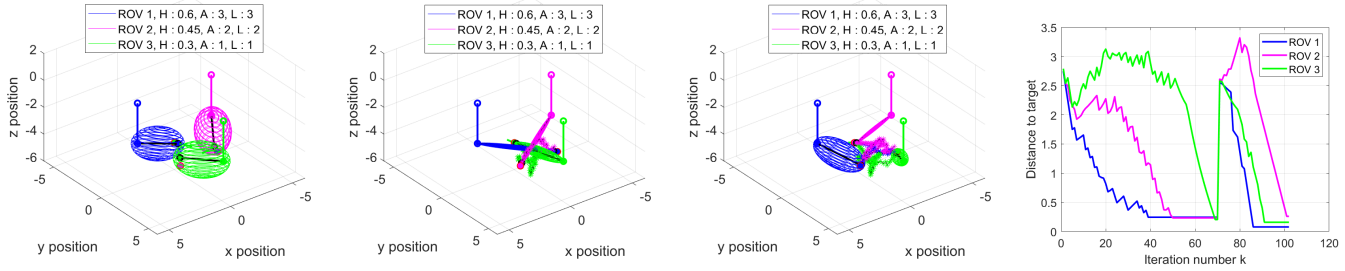

(g) Initial position (h) First target reached (i) Second target reached (j) Distance ROVs to current target

(j) Scenario of Figure 17a with addition of personality.

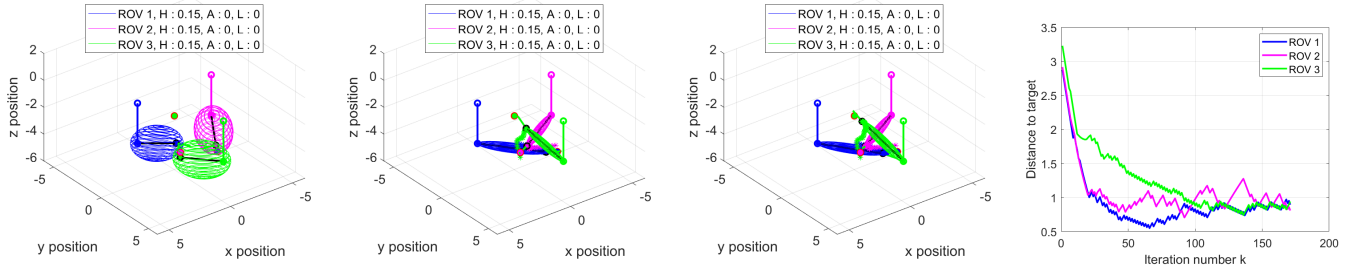

(l) Initial position (m) Going to the first target (n) Situation bloked (o) Distance ROVs to current target

(o) Three ROVs searching to reach crossed target. Intersection between ellipsoid $\mathcal{E}^L$ are not authorized: each ROVs are considered as a "full obstacle" by other. The situation is blocked and loop after $k > 100$, with no solution to unblock it.

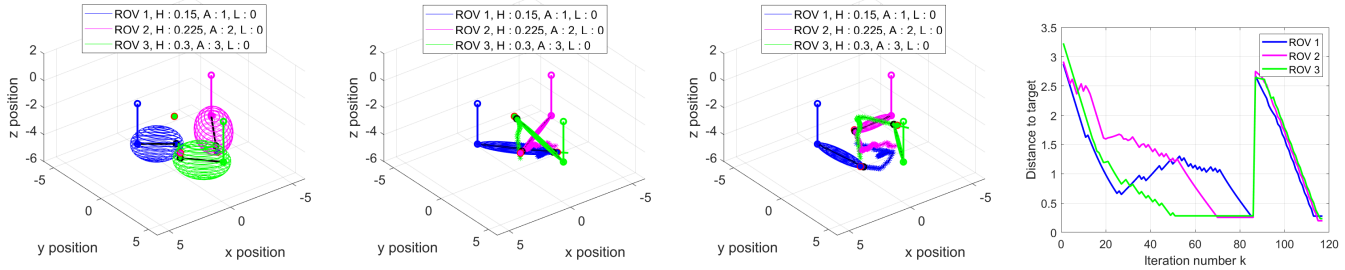

(q) Initial position (r) First target reached (s) Second target reached (t) Distance ROVs to current target

(t) Same scenario than in Figure 17k with personalities. A solution can be found.

Figure 17: Simulations with several ROVs.